



HAL
open science

Translational control of cell plasticity drives 5-FU tolerance

Mounira Chalabi-Dchar, Olivia Villeronce, Julie Ripoll, Anne Vincent, Tanguy Fenouil, Rita Khoueiry, Jérôme Kucharczak, Laura Jentschel, Frédéric Catez, Arnaud Vigneron, et al.

► **To cite this version:**

Mounira Chalabi-Dchar, Olivia Villeronce, Julie Ripoll, Anne Vincent, Tanguy Fenouil, et al.. Translational control of cell plasticity drives 5-FU tolerance. 2024. hal-04728612

HAL Id: hal-04728612

<https://hal.science/hal-04728612v1>

Preprint submitted on 9 Oct 2024

HAL is a multi-disciplinary open access archive for the deposit and dissemination of scientific research documents, whether they are published or not. The documents may come from teaching and research institutions in France or abroad, or from public or private research centers.

L'archive ouverte pluridisciplinaire **HAL**, est destinée au dépôt et à la diffusion de documents scientifiques de niveau recherche, publiés ou non, émanant des établissements d'enseignement et de recherche français ou étrangers, des laboratoires publics ou privés.

1
2
3
4
5
6
7
8
9
10
11
12
13
14
15
16
17
18
19
20
21
22
23
24
25
26
27
28
29
30
31
32
33
34
35
36
37
38
39

Translational control of cell plasticity drives 5-FU tolerance

Mounira Chalabi-Dchar ^{1, 16}, Olivia Villeronce ^{2, 16}, Julie Ripoll ^{3, 16}, Anne Vincent ¹, Tanguy Fenouil ^{1, 4, 5}, Rita Khoueiry ⁶, Jérôme Kucharczak ¹, Laura Jentschel ², Frédéric Catez ¹, Arnaud Vigneron ^{1, 7}, Julie Tréguier ², Céline Mandier ³, Céline Bouclier ², Jihane Vitre ², Louise Lagerqvist ², Armelle Choquet ², Zdenko Herceg ⁶, Christelle Machon ^{1, 8, 9}, Jérôme Guitton ^{1, 8, 9}, Alexandre David ^{10, 11}, Eric Solary ^{12, 13, 14}, David Bernard ^{1, 7, 14, 15}, Nadine Martin ^{1, 7, 14, 15}, Eric Rivals ^{3, 17}, Nicole Dalla Venezia ^{1, 17}, Julie Pannequin ^{2, 17}, Jean-Jacques Diaz ^{1, 7, 15, 17, 18, *}.

Affiliations

¹Centre de Recherche en Cancérologie de Lyon, INSERM U1052-CNRS UMR5286, Centre Léon Bérard, Université de Lyon, Université Claude Bernard Lyon1, 69008 Lyon, France

²IGF, University of Montpellier, CNRS, INSERM, Montpellier, France.

³LIRMM, Université Montpellier, CNRS, Montpellier, France

⁴Université Claude Bernard Lyon 1, Faculté de Médecine Lyon Est, Lyon, France

⁵Hospices Civils de Lyon, Groupement Hospitalier Est, Institut de Pathologie Multisite - Site Est, Bron, France

⁶Epigenomics and Mechanisms Branch, International Agency for Research on Cancer, World Health Organization, 69366 Cedex 07, Lyon, France

⁷Institut Convergence Plascan, Lyon, France.

⁸Biochemistry and Pharmaco-toxicology laboratory, Lyon Sud Hospital, University Hospital of Lyon, Pierre-Bénite, France

⁹ISPB Pharmacy Faculty of Lyon, University of Lyon, France

¹⁰IRCM, Univ Montpellier, ICM, INSERM, Montpellier 34090, France

¹¹IRMB-PPC, INM, Univ Montpellier, CHU Montpellier, INSERM CNRS, Montpellier 34295, France

¹²INSERM UMR 1287, Gustave Roussy, Villejuif France

¹³Université Paris-Saclay, Faculté de Médecine, Le Kremlin-Bicetre, France

¹⁴Equipe Labellisée « la Ligue Nationale Contre le Cancer », Lyon, France

¹⁵Labex Dev2Can, Lyon, France

¹⁶These authors contributed equally

¹⁷Senior Author

¹⁸Lead Contact

*Corresponding author: jean-jacques.diaz@lyon.unicancer.fr

40 **Abstract**

41

42

43 All routine clinical treatments for colorectal cancer include 5-fluorouracil (5-FU), which cannot
44 counteract recurrence and metastases formation. As the pyrimidine analog 5-FU can impact
45 multiple pathways including both DNA and RNA metabolism, studying its mode of actions could
46 lead to improved therapies. Using a dedicated reporter system for lineage-tracing and deep
47 translome profiling we demonstrate that 5-FU causes some colorectal cancer cells to tolerate
48 the drug, due to a durable translational reprogramming that sustains cell plasticity. This period
49 of drug tolerance coincides with specific translational activation of genes coding for proteins
50 with major pro-tumoral functions. We unravel a major unexpected translational overexpression
51 of the pro-inflammatory and pro-tumoral IL-8 cytokine, alongside other anti-apoptotic,
52 senescence-associated secretory phenotype and cancer-related senescence phenotype
53 genes. Given the adverse prognostic implications of elevated IL-8 levels across various
54 cancers, our findings suggest IL-8 targeting could counteract 5-FU resistance.

55

56

57 **Keywords**

58 Drug-tolerance, Translational regulation, Ribosome, Persister cells, SASP, Colorectal cancers,
59 Translatomics, 5-Fluorouracil

60

61

62

63 Introduction

64
65 Chemotherapeutic regimens constitute a cornerstone in the management of solid tumors,
66 including those affecting the digestive tract, with fluoropyrimidines, such as 5-Fluorouracil (5-
67 FU) or capecitabine, being key components for over six decades ¹. Colorectal cancer (CRC)
68 is the second most common cause of cancer-related deaths in western countries with annual
69 worldwide incidence and mortality rates near 2 million and 1 million cases respectively ^{2, 3}.
70 Fluoropyrimidines are part of first-line adjuvant therapies for CRC with most of the patients
71 from high-risk stage II to stage IV receiving a regimen containing these drugs. To date,
72 fluoropyrimidines are used alone for patients over 70 or for some high-risk stage II patients.
73 For other patients they are combined with other molecules (oxaliplatin, irinotecan, and targeted
74 therapies including bevacizumab, cetuximab or panitumumab). Fluoropyrimidine treatment
75 contributes to just a 10% increase in 8-year overall survival ⁴. Consequently, there is a critical
76 need to enhance the effectiveness of treatments utilizing 5-FU. Surprisingly, despite being one
77 of the oldest and most widely used chemotherapeutic drugs, some aspects of its mode of
78 action remain unclear. This is especially true in deciphering the molecular mechanisms
79 underlying emergence of a specific population of tumor cells, named persisters, that survive
80 exposure to fluoropyrimidines and contribute to acquired resistance and recurrence of the
81 cancer disease. These cells constitute one of the major challenges in cancer biology to
82 optimize routine treatments to prevent drug escape, metastasis formation and recurrence ⁵⁻⁷.

83
84 5-FU is considered as an antimetabolite that exerts its cytotoxicity through its three active
85 metabolites that are 5-fluorodeoxyuridine monophosphate (5-FdUMP), 5-fluorodeoxyuridine
86 triphosphate (5-FdUTP), and 5-fluorouridine triphosphate (5-FUTP). The 5-FdUMP and 5-
87 FdUTP metabolites confer to 5-FU its ability to affect a variety of DNA-based mechanisms ¹.
88 Its capacity to arrest DNA replication ^{8, 9}, to induce DNA damage and to alter DNA repair ¹⁰⁻¹²
89 undoubtedly contribute to the cytotoxic effects and cell death. It is now firmly established that
90 5-FU cytotoxicity is also due to its ability to alter all RNA-based biochemical pathways ¹³
91 through 5-FU incorporation into RNA ¹⁴, RNA metabolism inhibition ¹⁵ and ribosome biogenesis
92 alteration ¹⁶. Several groups, including our own, have shed light on how 5-FU integrates into
93 ribosomal RNA (rRNA), revealing an unexpected contribution of this biochemical pathway to
94 therapeutic escape ^{13, 17, 18}.

95
96 Current knowledge on the impact of 5-FU on gene expression relies essentially on
97 transcriptional profiling ¹⁹⁻²⁴. However, recent evidence indicates that 5-FU also affects
98 translational efficiency and fidelity ^{18, 25-28}. Nevertheless, the impact of 5-FU treatment on the
99 dynamics of translation rewiring and its consequences on treated cells remain to be explored.

100
101 Here we used polysome profiling to monitor CRC cells following 5-FU treatment. Through
102 translational analysis, we identified a dynamic and comprehensive modification in the gene
103 expression of persister cells. Further we pinpoint proteins whose synthesis defies the general
104 shutdown of protein synthesis induced by 5-FU. Contrary to previous assumptions we find
105 strikingly that some gene expression is actually upregulated by 5-FU treatment rather than
106 being suppressed. Moreover, we identified among these genes some that promote cell survival
107 and cell plasticity through the senescence-associated secretory phenotype (SASP),
108 contributing to the long-term detrimental effects of 5-FU.

111
112
113
114
115
116
117
118
119
120
121
122
123
124
125
126
127
128
129
130
131
132
133
134
135
136
137
138
139
140
141
142
143
144
145
146
147
148
149
150
151
152
153
154
155
156
157
158

Results

5-FU induces plasticity of cancer cells escaping 5-FU-induced death

To investigate the impact of 5-FU on colorectal cancer (CRC) cells, we used two CRC cell lines, HCT-116 and HT-29, representative of the two main subtypes of CRC exhibiting different genotypes, including the *TP53* status and the microsatellite stability status (Extended Data Fig. 1a). We treated HCT-116 and HT-29 cells with a clinically relevant concentration of 10 μ M 5-FU for two and three days respectively^{29,30}. Cell number was then monitored over seven days. An experimental schema is given in Extended Data Fig. 1b. As expected, without treatment, the number of cells increased steadily, whereas 5-FU treatment kept the cell number in check (Fig. 1a). This treatment would be expected to lead the cells to eventually die by apoptosis¹. However, by seven days, up to 40% - 50% of the initial number of cells escaped 5-FU-induced apoptosis (Fig. 1b). For further exploration into the proportion of cells resisting cell death, we tracked the dying cells at five time points by trypan blue-exclusion test. Around half of the HCT-116 cells remained viable at day 5 (D5) and D7 (Extended Data Fig. 1c). This increase of cell death coincides with induction of P53 and its phosphorylation at Serine 46 (Extended Data Fig. 1d), modification known to enhance the transactivation of a specific group of its pro-apoptotic target genes³¹. Similarly, while *TP53*-defective HT-29 cells died in the same proportions at D7, HT-29 underwent a delayed cell death in the early stages of treatment (D1 to D5) (Extended Data Fig. 1c). Flow cytometry monitoring the proportion of HCT-116 cells that exhibited cleaved-caspase 3 apoptotic marker showed that 5-FU induced modest apoptosis in the first two days of treatment, which increased dramatically at D7 (Fig. 1c). The sub G0/G1 fraction, representing fragmented DNA content of apoptotic cells, increased four-fold after 5-FU treatment, suggesting that early caspase 3 activation precedes cell death (Extended Data Fig. 1e). These results indicated that while an apoptotic death program was induced by 5-FU treatment, nearly half of the cells were persisters, that had escaped the apoptotic process at D7.

To investigate whether 5-FU CRC cell resistance to apoptosis is induced by plasticity, we used a conventional test based on the lentiviral pGreenZeo Reporter Vector. In this vector, the expression of the green fluorescent protein (GFP) is under the control of the *NANOG* promoter. The expression of *NANOG* is commonly associated with either pluripotency, stemness or EMT, themselves strongly linked to cell plasticity³²⁻³⁴. Hence, a readout for cell plasticity phenotype was achieved by exposing transduced cells to 5-FU and measuring the number of cells highly expressing GFP, called GFP^{high} cells. To validate the experimental system, we first analyzed the expression of *NANOG* protein and GFP by immunofluorescence in HT-29 cells (Extended Data Fig. 1f). The level of both proteins increased in parallel in treated cells (Extended Data Fig. 1g). Then, using fluorescence-activated cell sorting (FACS) analysis of the HCT-116 and HT-29 cells, we found that the percentage of GFP^{high} cells increased by 4 and 6-fold upon 5-FU treatment, respectively, suggesting 5-FU induced cell plasticity. Although this cell population reduced slightly after 5-FU withdrawal, their numbers remained higher for several days (Fig. 1d). To further investigate the impact of 5-FU treatment on cell plasticity, we assessed its ability to stimulate the *NANOG* promoter in an animal model. We designed a model of HCT-116 or HT-29 subcutaneously xenografted in nude mice and treated with 5-FU, then we monitored the proportion of GFP^{high} cells within their tumors. The tumors isolated from mice subjected to 5-FU treatment were enriched in GFP^{high} cells by 3.5-fold and 2.4-fold in HCT-116 and HT-29 models respectively (Fig. 1e).

159
160 Next, the aim was to determine whether the increased proportion of GFP^{high} cells observed
161 upon 5-FU treatment reflects an enrichment of the existing GFP^{high} cells and/or a
162 reprogramming of the initial GFP^{low} cells into GFP^{high} cells (plasticity). We therefore established
163 a dedicated reporter system for lineage-tracing populations (Fig. 1f). In essence, naive CRC
164 cells containing a low basal percentage of GFP^{high} cells were transduced with either pLenti-
165 EIF1 α -AmCyan (AmCyan cells) or pLenti-EIF1 α -mCherry (mCherry cells) lentiviral vector.
166 After sorting mCherry cells strongly expressing GFP (GFP^{high}mCherry cells) and AmCyan cells
167 poorly expressing GFP (GFP^{low}AmCyan cells) separately, the two populations were pooled at
168 the same ratio as the original cell line to be treated with 5-FU for the indicated time. The GFP^{high}
169 cells were analyzed by flow cytometry to discriminate between enrichment (increase of the
170 pre-existing mCherry cell population compared with control cells) and reprogramming
171 (appearance of AmCyan cell population that was absent from the pooled population before
172 treatment). Surprisingly, analysis of GFP^{high}AmCyan cells showed that the proportion of
173 GFP^{high}AmCyan cells in control population increased around six-fold in treated cells (Fig. 1g,h
174 and Extended Data Fig. 1h). These results indicate that GFP^{high} cells can arise from GFP^{low}
175 cells upon 5-FU treatment, contributing to cancer cell plasticity.

176

177 **5-FU reshapes the translational program of persister cells**

178 We recently discovered that, after a single day of 5-FU treatment, cells produce fluorinated
179 ribosomes (F-ribosomes), causing a major reprogramming of translation ¹⁸. To study this
180 phenomenon over a longer time course, we monitored the F-ribosomes content in CRC cells,
181 after two days of 5-FU treatment up until the arrival of persister cells at D7. There was a
182 significant sustained enrichment of F-ribosomes in both cell lines (Fig. 2a). For example, in
183 HCT-116 cells, number of 5-FU molecules *per* ribosome increased from 7 at D1 to 11 at D2
184 and reached a maximum of 19 *per* ribosome at D7, indicating that persister cells at D7
185 contained heavily fluorinated ribosomes.

186

187 To examine the progression of the initial 5-FU-induced translational reprogramming beyond
188 the 24-hour treatment period ^{18, 35}, we explored translational changes arising throughout the
189 course of treatment by polysome profiling. As translation is a cytoplasmic event, we first
190 analyzed the RNAs isolated from the cytoplasmic cellular fraction (Extended Data Fig. 2a).
191 RNA sequencing (RNA-seq) detected 15,891 cytoplasmic RNA, of which 2,364, 3,140 and
192 4,242 (corresponding to 15%, 20%, and 27% of detected RNAs) were differentially present in
193 treated cells at D1, D2 and D7 respectively (Fig. 2b). The amounts of cytoplasmic RNAs reflect
194 their rates of synthesis, post-transcriptional processing, transport and stability, meaning that
195 they do not reflect transcription only. To dissect the effect of 5-FU on translational control, we
196 compared the overall cytoplasmic RNA content with the cytoplasmic RNA being associated
197 with actively translating ribosomes (*i.e.* polysomes). There was a strikingly different pattern
198 from cytoplasmic RNA. For polysomal RNAs, the numbers were 1,226, 3,602 and 2,906 (*i.e.*
199 8%, 23% and 18%) at the D1, D2 and D7 time points respectively (Fig. 2b). Most notable was
200 a striking 3-fold increase in polysomal RNA between D1 and D2, which reduced at D7 while
201 total cytoplasmic RNA was still increasing. Consistently, principal component analysis (PCA)
202 underscored significant differences between conditions (Extended Data Fig. 2b). The first axis
203 strongly differentiated polysomal RNA from cytoplasmic RNA, irrespective of the day of
204 treatment. The second and third axes strongly differentiated D0 from all days of treatment, and
205 differentiated D7 from D1 and D2 time points, indicating that the translational landscape of the
206 cells changed during the time course. A Gene Ontology (GO) enrichment analysis of

207 cytoplasmic total mRNA revealed that catabolism, stress response, and ribosome were
208 significantly enriched at D1, D2 and D7 respectively. The picture for actively translated genes,
209 i.e. in polysomes, was completely different. At D1 of treatment there was enrichment of
210 nucleosome organization. By D2 the changes had shifted to genes involved in RNA processing
211 and to RNA export from the nucleus at D7. Other translation-related mechanisms including
212 tRNA pathways were also significantly enriched at D7 (Fig. 2c).
213 Altogether these data highlight the differential impact of 5-FU on the amount of RNA in the
214 cytoplasm and the recruitment of RNAs to polysomes.

215
216 To better characterize the response to 5-FU treatment at the translational level, we next
217 focused on the variations in the amount of individual RNA within the polysomal fraction.
218 Consistent with the PCA, most of the polysomal RNAs from D1 continued to be differentially
219 associated with polysomes at D2. Furthermore, the numbers of polysomal RNAs that are only
220 deregulated at D2 was 8-fold greater than at D1 (1,635 at D2 vs 196 at D1) (Fig. 2d). These
221 data suggested that the translational reprogramming induced by 5-FU during treatment highly
222 differed from that observed five days after treatment. Among the RNAs being translationally
223 altered, we found that 68%, 49% and 51% of them were upregulated at the three D1, D2 and
224 D7 timepoints respectively (Fig. 2e). This observation highlights that although commonly
225 considered as a down-regulator of the whole gene expression landscape, 5-FU unexpectedly
226 upregulates the translation of many genes.

227

228 **5-FU modifies the translation of epigenetic regulator genes**

229 We next determined how 5-FU-induced translational reprogramming enabled cells to escape
230 treatment. We initially focused on epigenetic regulator genes (ERGs) highly involved in cell
231 plasticity in the literature. ERGs play a major role in the early steps of gene expression by
232 regulating processes, including DNA methylation, chromatin remodeling and histone
233 modifications. This is required for the establishment and the maintenance of cell identity and,
234 as such, ERGs are key contributors to cancer cell plasticity^{36,37}. We used the well-defined list
235 of 426 genes³⁸ representing the main ERGs coding for histone modifiers, DNA methylation
236 regulators, chromatin remodelers, helicases, and other epigenetic entities to determine which
237 of the major ERGs are translationally regulated by 5-FU.

238 GO enrichment analysis showed that, among RNA whose association with polysomes was
239 modified, those involved in nucleosome related mechanisms were the most represented at D1
240 (Fig. 2c). This suggests a strong and rapid functional effect of 5-FU on nucleosome remodeling,
241 in connection with ERG-induced chromatin changes, expected to modify the epigenome. Over
242 a third, 124 of the global list of 426 ERGs, was translationally deregulated over time (Fig. 3a,b
243 and Extended Data Table 1). The number of differentially translated ERGs in treated cells
244 increased near 6-fold between D1 and D2 and slightly decreased after 5-FU withdrawal (79 at
245 D7 vs 93 at D2). While 60% of the differentially translated ERGs were commonly deregulated
246 at D2 and D7, around 40% of them were specifically deregulated at these time points. Among
247 the 124 translationally deregulated ERGs, 109 ERGs were downregulated while only 15 ERGs
248 were upregulated, representing 88% and 12% of all deregulated ERGs respectively (Fig. 3c
249 and Extended Data Table 2 and Table 3). This is a vastly different pattern than for the totality
250 of translationally regulated genes at D7 which were approximately half downregulated RNAs
251 and half upregulated (Fig. 2e). Altogether, these data highlight the dynamic and specific
252 translational control of ERGs expression following 5-FU treatment.

253

254 Among the numerous downregulated genes were many histone methylation regulators,
255 including writers (i.e. EZH2, SETD1B, and PRDM16), erasers (i.e. KDM2A, KDM5A, and
256 KDM7A) and readers (i.e. CBX5). At D2 and D7 there was downregulation of the DNA
257 methylation writers DNMT1 and DNMT3, along with the decreased expression of TET
258 demethylating enzymes and MBD3 writer. Many histone acetylation regulators, known to play
259 a role in regulating chromatin accessibility and gene expression, were deregulated at different
260 time points, including histone acetyltransferases (i.e. KAT5 and KAT8) and histone
261 deacetylases (i.e. HDAC4 and HDAC6) that were downregulated (Fig. 3d), while some histone
262 deacetylases (i.e. SIRT2 and SIRT4) were upregulated.

263 We observed a fascinating pattern in acetylation modifiers at D7. As with ERGs in general,
264 many histone acetylation regulators were downregulated at this time point, including histone
265 acetyltransferases KAT5 and KAT8 and histone acetylation enhancers EP300, EP400, and
266 SRCAP. At the same time, at D7, there was a substantial translational upregulation of histone
267 deacetylase HDAC9. These observations suggest a coordinated 5-FU-induced decrease in
268 translation of histone acetylators at D7.

269
270 Among the 29 ERGs that were deregulated in persister cells, three ERGs were specifically
271 upregulated, the most prominent being HDAC9. While the engagement of HDAC9 mRNA
272 within polysomes remained unchanged during treatment (D1 and D2), it significantly increased
273 by four-fold at D7 compared to untreated cells (D0 time point). Monitoring of HDAC9 protein
274 quantity by western blotting confirmed this translational upregulation observed at D7 (Fig. 3d).
275 This sudden elevated efficiency of translational activity was accompanied by a moderate
276 increase of the mRNA level in cytoplasm. These data suggest that the increase of HDAC9
277 expression in persister cells is mainly driven by an active translational mechanism.

278 Altogether, the global translational changes of ERGs support the idea of a dynamic epigenetic
279 response of cells upon 5-FU treatment over time, reflecting the contribution of epigenetic-
280 driven cell state plasticity.

281

282 **5-FU induces cell death program and cell cycle arrest at the translational level**

283 Since a significant percentage of cells escape the 5-FU-induced cell death and persist for up
284 to seven days (with a maximum of 40% to 50%), we determined whether a translational switch
285 of apoptosis-related genes occurs in response to 5-FU treatment. We analyzed the
286 translome data focusing on genes known to be specifically involved in cell death. Out of the
287 85 apoptotic genes (from <http://deathbase.org>), 32 genes were translationally up-regulated in
288 response to 5-FU (Extended Data Fig. 3a). Strikingly, genes that were translationally
289 upregulated at the outset of the treatment (D1) and maintained up to D7 were, in a vast
290 majority, pro-apoptotic factors. This included genes encoding pro-apoptotic proteins of the
291 BCL2 family including the BH3-only proteins PUMA (encoded by *BBC3*), NOXA (encoded by
292 *PMAIP1*) and BIK, as well as the multi-domain effector BAX, all of which known to be P53-
293 inducible proapoptotic genes³¹. Furthermore, the translation levels of certain death receptors
294 involved in the extrinsic pathway of apoptosis, including FAS (*TNFRSF6*), TRAIL-R1
295 (*TNFRSF10a*) and TRAIL-R2 (*TNFRSF10b*), were similarly upregulated during the early days
296 of treatment and maintained up to D7 for FAS (Fig. 4a). However, this robust pro-apoptotic
297 signature contrasts with the upregulation of TRAIL-R3 (*TNFRSF10c*), a decoy receptor lacking
298 a functional intracytoplasmic domain known to protect cells from TRAIL-induced apoptosis by
299 interfering with the binding of the pro-apoptotic TRAIL-R1 and TRAIL-R2. Consequently, the
300 sharp translational upregulation of TRAIL-R3 from D1 to D7 may significantly mitigate TRAIL-
301 R1 and TRAIL-R2-induced apoptosis during the early stages of treatment. Interestingly, the

302 pro-survival factor cIAP2, encoded by *BIRC3*, which serves as a potent inhibitor of both the
303 extrinsic and intrinsic pathways of apoptosis, exhibits increased translation levels from D1 up
304 to D7. It, along with TRAIL-R3, represents anti-apoptotic candidates exerting protective activity
305 throughout the course of 5-FU treatment (Fig. 4a).

306
307 Next, we tested these findings at the protein level and found that the expression of two pro-
308 apoptotic proteins, NOXA and BAX, were induced and maintained up to D7 after 5-FU
309 treatment in HCT-116 cells. The same trend of induction was observed with pro-survival cIAP2,
310 the expression of which increased from the first day of 5-FU treatment in HCT-116 cells (Fig.
311 4b). Similarly, 5-FU induced cIAP2 expression in HT-29 cells, with a marked late accumulation
312 of the protein at D7, while both pro-apoptotic proteins NOXA and BAX decreases at this time
313 point (Fig. 4c). Altogether, these results suggest that 5-FU drives translation reprogramming
314 in CRC cells. Regulated targets include both pro-apoptotic inducers and a unique anti-
315 apoptotic factor, that likely underlies the cell phenotype with broad involvement in cell death
316 and survival.

317
318 Since previous work showed that a 24h treatment with clinically relevant doses of 5-FU induces
319 cell cycle arrest^{24, 35}, we investigated the capacity of 5-FU to alter the cell cycle over a longer
320 period of time. Thus, we analyzed propidium iodide (PI) incorporation into DNA by flow
321 cytometry and evaluated HCT-116 cell distribution, in each active phase of the cell cycle,
322 according to their DNA content. As expected, untreated cells (D0) were asynchronous, with
323 approximately half of cells in S phase and approximately a quarter each in G0/G1 and G2/M
324 phases (Fig. 4d,e). In contrast, cells treated with 5-FU were arrested in the G1/S transition at
325 D1 and they remained arrested throughout the seven days even after treatment withdrawal.
326 Cells that were already in S phase at D0 continued cycling by entering either in a new G1
327 phase, or dying. Therefore, most HCT-116 cells were blocked in G1 phase (49.2% of cells in
328 G0/G1 phase at D7 vs 26.5% at D0).

329 Similarly, treatment with 5-FU led to cell cycle arrest of HT-29 cells that are mutated for *TP53*
330³⁹. While non-treated cells were characterized by an asynchronous cell cycle the 5-FU treated
331 cells displayed no accumulation in G2/M phase from D1 up to D7, regardless of the increase
332 in the proportion of cells in G1 and S phases (Fig. 4f,g).

333
334 To determine whether the 5-FU-driven translational reprogramming sustained the cell cycle
335 arrest, we performed gene set enrichment analysis comparing cells at D7 with untreated cells
336 (D0) using polysomal RNA data from translome data. This unveiled negative enrichment of
337 gene sets associated with the cell cycle (Fig. 4h). To investigate whether the cell cycle arrest
338 resulted from a translational control of cell cycle effectors, we analyzed data from the HCT-
339 116 translome. Importantly, genes encoding D-, E-, A- and B-type cyclins showed an altered
340 translational regulation during and after treatment (Extended Data Fig. 3b). The *CCND1* gene
341 (encoding cyclin D1) was translationally upregulated at D2 and maintained upregulated up to
342 D7, in line with cell cycle arrest in G1 phase. Meanwhile, *CCNA2* and *CCNB1* genes (encoding
343 cyclin A2 and cyclin B1 respectively) were translationally downregulated at D2, in agreement
344 with the observed completion of cycles during global cycle arrest. These data thus indicate
345 that 5-FU treatment induces cell cycle arrest, at least in part, through the translational
346 regulation of key cell cycle factors.

347
348 To further test our findings, the expression of the cell cycle factors was assessed by western
349 blotting (Fig. 4i). Indeed, cyclin D1 and its CDK4 cofactor increased progressively from D1 to

350 D2 and were maintained upregulated after 5-FU treatment (D5), while the expression of cyclin
351 A and cyclin B together with the phosphorylation of CDK1 on Tyrosine 15 decreased from D1
352 to D2, and were maintained at a low level up to D5. These findings further confirm that 5-FU
353 alters translation of essential cell cycle factors, leading to simultaneous arrest in the G1 phase.
354 Next, we assessed the phosphorylation of histone H3 at Serine 10, a specific marker of mitotic
355 cells (Fig. 4j). In HCT-116 there was a sharp decrease in the phosphorylation of H3 from D1
356 to D7 after 5-FU treatment, suggesting an absence of mitosis. As the G1/S transition is highly
357 controlled by the P53-inducible P21 effector, to halt the cell cycle in response to DNA damage,
358 we examined the translation of CDKN1A that encodes P21 upon 5-FU exposure. The
359 translation of CDKN1A increased during treatment and was maintained at high levels
360 (Extended Data Fig. 3b), which parallels P53 increased expression at the same time point of
361 treatment (Extended Data Fig. 1d). We further verified the overexpression of P21 by western
362 blotting (Fig. 4j). Interestingly, the phosphorylation of H3 and the expression of P21 varied
363 through the same trends in HT-29 cells although with different kinetics and intensity according
364 to the mutated status of *TP53* in HT-29 cells (Fig. 4k).

365

366 Altogether, 5-FU induced a translation-dependent alteration of essential cell cycle factors
367 leading to prolonged cell cycle arrest of persister cells, which was sustained by increased
368 expression of master cell cycle inhibitor P21 independently of mutational status of *TP53*.

369

370 **5-FU induces a translomic signature in SASP related genes**

371 The strong cycle arrest in HCT-116 and HT-29 persister cells observed several days after 5-
372 FU removal is reminiscent of a senescence signature⁴⁰. Therefore, we further explored
373 whether cells initiated a senescent process. A detailed analysis of cell morphology showed
374 that both cell lines displayed an enlarged size during 5-FU treatment and were characterized
375 by irregular and various shapes after 5-FU withdrawal with cytoplasmic droplets, a common
376 feature of senescent cells (Extended Data Fig. 4a,b). The increased activity of the lysosomal
377 enzyme, the senescence-associated beta-galactosidase (SA-beta-gal), is among the most
378 frequently measured markers of senescent cells⁴¹. An accumulation of blue-stained SA-beta-
379 gal positive cells in HCT-116 persister cells compared to untreated cells (Fig. 5a,b) validated
380 that senescence was induced by 5-FU and persisted 5 days beyond the treatment.

381

382 To determine whether the 5-FU-driven senescence program was driven by translational
383 reprogramming, we performed GSEA comparing cells at D7 with untreated cells (D0) using the
384 polysomal RNA data from translome data. This unveiled positive enrichment of gene sets
385 associated with senescence and the SASP, and simultaneously, an under-representation of
386 genes involved in DNA repair, a characteristic feature of senescent cells⁴², further confirming
387 the senescence trait of persister cells at D7 (Fig. 5c).

388

389 To test if the senescence program resulted from translational control, we analyzed data from
390 the translome and focused on genes that regulate DNA repair, Lamin B1 and SASP. First,
391 DNA repair factors, RAD51, RFC4, BRCA1, BLM, and POLE2, were all translationally
392 downregulated, at D1 and/or D2 (Extended Data Fig. 4c). Lamin B1, whose reduced level is a
393 trait of senescent cells⁴³, was translationally downregulated immediately upon treatment
394 initiation (Extended Data Fig. 4c). Then, we focused on genes known to be involved in SASP,
395 including conventional SASP-related genes^{44, 45} and cancer-related SASP factors⁴⁶⁻⁴⁹. Out of
396 the 38 SASP-related genes, extracted from the translome data, 27 genes displayed an
397 altered translational regulation with 24 being upregulated, indicative of a strong SASP

398 signature (Fig. 5d). A detailed analysis of the translation of these genes showed that the *NRG1*
399 growth factor and the *CXCL1*, *CXCL3*, and *CXCL8* proinflammatory genes, were progressively
400 upregulated through treatment, with a maximum at D7.

401 Altogether, these data showed that persister cells exhibit a senescent phenotype sustained by
402 translational upregulation of mRNAs associated with SASP, including mRNAs encoding
403 inflammatory cytokines.

404

405 To emphasize the importance of 5-FU driven translational deregulation of these cytokines, we
406 categorized their corresponding mRNAs as follows: those exhibiting changes in cytoplasm
407 levels representing an integration of their rates of synthesis, post-transcriptional processing,
408 transport and stability, and those showing changes in polysomal fractions representing
409 changes in their translational efficiency (Fig. 5e). Engagement of the three mRNAs coding for
410 *CXCL3*, *CXCL1* and *CXCL8* within polysomes increased regularly from D1 to D7. In addition,
411 the increase of mRNA engaged into polysomes over time (from D1 to D7) was slightly higher
412 than that the increase in the cytoplasm for *CXCL1* and *CXCL8*, supporting the notion that
413 active translational mechanism can drive the increase of *CXCL1* and *CXCL8* synthesis and
414 secretion, and to a lesser extent that of *CXCL3*.

415 Protein-level monitoring was conducted by ELISA to validate the translational upregulation of
416 the three translationally upregulated cytokines, *CXCL3*, *CXCL1*, and IL-8 (encoded by
417 *CXCL8*). The culture medium from HCT-116 cells at D7 revealed a strong increase in their
418 secretion by persister cells following 5-FU treatment by 11, 17, and 37-fold, respectively (Fig.
419 5f).

420

421 **IL-8 overexpression contributes to treatment escape and provides protumoral** 422 **capacities to persister cells**

423 Next, we sought to establish the role of some of the three translationally upregulated cytokines.
424 We were immediately attracted to IL-8, encoded by *CXCL8*, as it exhibits major pro-tumoral
425 pleiotropic activities^{50, 51}. Furthermore, of the three, *CXCL3* modulation was limited (Fig. 5e).
426 Then, *CXCL1* has a potentially similar role to *CXCL8*, as it binds to a common receptor CXCR2
427 and it also cooperates with IL-8⁵². We therefore focused on the *CXCL8* gene among the three
428 cytokine genes (*CXCL3*, *CXCL1* and *CXCL8*) whose translational efficiency was upregulated
429 by 5-FU.

430

431 To determine whether IL-8 was required for the emergence and selection of persister cells
432 exhibiting plasticity, following 5-FU treatment, we either depleted its expression or inhibited its
433 activity by using siRNA and reparixin, respectively. As a read out for cell plasticity, we assessed
434 the ability to form spheres at different times following 5-FU treatment (Extended Data Fig. 5a).
435 There was a sharp decrease of *CXCL8* mRNA and IL-8 secreted protein induced by siRNA
436 targeting *CXCL8* (Extended Data Fig. 5b,c). This was accompanied by a significant 2.1-fold
437 reduction of the sphere frequency observed at D7 as well as at D16 (Fig. 6a). Furthermore,
438 inhibition of IL-8 receptors with reparixin had a similar effect with a near halving of sphere
439 frequency (Fig. 6b).

440 In parallel, we investigated whether targeting IL-8 could affect the viability of persister cells. As
441 shown in Fig. 6c, cells transfected with siRNA targeting IL-8 exhibited a 2.7- and 3.7-fold lower
442 viability, respectively at D7 and D10 compared to cells transfected with control siRNA.
443 Similarly, treatment with reparixin also reduced the viability of persister cells, by 2.5-fold at D7,
444 this effect being amplified at D10 with a 4.6- fold decreased viability (Fig. 6d). Altogether these

445 data showed that increase of translational efficiency of CXCL8 induced by 5-FU was necessary
446 for the survival of cells exhibiting plasticity, acknowledged as persister cells.
447

448

449 **Discussion**

450

451 We have shown here that 5FU treatment of colorectal cancer cells induces a translational
452 reprogramming sustaining cell plasticity. This translational reprogramming includes genes of
453 the SASP, of which CXCL8 might be highly relevant by promoting the generation of persister
454 cells.

455 Identifying the molecular mechanisms sustaining resistance to treatment used routinely in
456 clinic, notably for the management of CRC patients, is one of the major challenges of cancer
457 biology^{53,54}. Because it was known that some CRC cells escape 5-FU treatment and become
458 resistant (Boumahdi and de Sauvage, 2020; Kemper et al., 2014; Rambow et al., 2018), and
459 because we previously demonstrated that cells treated with 5-FU produce fluorinated
460 ribosomes that are responsible for a major translational reprogramming¹⁸, we asked whether
461 this non-genetic process could contribute to the emergence of so-called persister cells⁵. These
462 cells are now recognized as a reservoir of cells that are prone to drive tumor progression,
463 namely recurrence and metastasis formation^{5,7}. Using a deep polysome profiling approach,
464 we monitored the 5-FU-induced translational reprogramming to identify translational switch
465 occurring in genes playing a key role in the establishment of the tolerant phenotype. Only a
466 few large-scale reports have investigated whether 5-FU could affect the whole cellular
467 translome. Two previous polysome profiling studies of cellular models suggested that 5-FU
468 could regulate the translation of a set of mRNAs^{55,56}. Studies from our laboratory showed that
469 5-FU modifies the translome signature of cells under treatment^{18,35}. Here, we discovered
470 that near 20% of all cellular RNA analyzed were subjected to translational regulation in
471 persister cells, and that half of them were upregulated. This means that some cells undergo
472 an active protein synthesis, even though the overall population faces cell cycle arrest. This
473 large-scale upregulation of translation was unexpected because of the extensively
474 documented pleiotropic inhibitory effects of 5-FU on most of the fundamental processes of cell
475 biology, and particularly on ribosome biogenesis and metabolism of DNA and RNA^{1,13}.

476

477 While 5-FU was initially described for its deleterious effect on DNA, numerous studies clearly
478 established that its cytotoxicity was also largely due to its integration into RNA^{13,15,57-59}. It is
479 therefore possible that RNA could titrate the available cellular pool of 5-FU thus enabling cells
480 to escape the DNA-driven cytotoxicity. However, the price to pay is a major modification of
481 gene expression due to the production of fluorinated ribosomes, which in turn promote the
482 expression of survival genes¹⁸. Overall, this highlights that 5-FU-driven ribosome plasticity
483 contributes to plasticity of the cell itself.

484

485 Cell plasticity is an intrinsic cellular property, which engenders an adaptive and transient non-
486 genetic cellular response, enabling evasion of a vast variety of stresses. In the context of
487 cancers, cell plasticity facilitates drug evasion, through non-genetic mechanisms. By
488 challenging cell plasticity over long periods of time, therapies ultimately render a proportion of
489 cells both more invasive and resistant to anti-cancer therapies⁶⁰⁻⁶². Here, thanks to the
490 establishment of a unique reporter system for lineage-tracing we showed not only that by killing

491 sensitive cells, 5-FU enriches pre-existing tolerant cells, but also that 5-FU induces a
492 reprogramming of sensitive cells by a novel translational control mechanism.

493

494 Our translome analysis revealed the deregulation of approximately 30% of the main 426
495 epigenetic regulators of chromatin states. Both negative and positive regulators of histone and
496 DNA epigenetic marks were expressed differently upon treatment. These extensive changes
497 in ERG translation were mostly pronounced in persister cells. This attests to an important
498 chromatin dynamic remodeling during treatment, sustaining 5-FU driven cell plasticity, as being
499 responsible for the persister phenotype. Chromatin plasticity is key in the development of many
500 cancers, including CRC, and it involves the acquisition of a stem-like cell state^{63, 64}. Moreover,
501 alterations in chromatin regulatory proteins have been reported to confer resistance to targeted
502 therapeutic agents, by regulating cell plasticity^{37, 65, 66}.

503

504 Analysis of global chromatin accessibility, by ATAC-seq technology in a model of 5-FU-
505 resistant CRC HCT-15 cells, showed that 5-FU resistant cells display a different epigenetic
506 landscape compared to their parental cells⁶⁷. Here, we show for the first time that 5-FU alters
507 expression of ERGs at the translational level. Among the 29 ERGs that were translationally
508 deregulated in persister cells, three were specifically upregulated, the most upregulated one
509 being HDAC9. This supports the notion that this protein may contribute the 5-FU-tolerant
510 phenotype of persister cells. Members of HDAC family are epigenetic modifiers acting on the
511 dynamic regulation of acetylation of histones, the major structural proteins associated with
512 DNA to constitute the chromatin⁶⁸. Clinically, HDAC9 was found highly expressed in B-cell
513 lymphomas, serous ovarian and gastric cancers⁶⁹⁻⁷¹, and silencing of HDAC9 in SKOV3
514 serous ovarian cells decreased their migrating properties and inhibited the expression of EMT-
515 related genes, supporting a role for HDAC9 in cancer progression and aggressiveness⁷⁰. Here
516 we implicate HDAC9 in cell plasticity. An association between high expression of HDAC9 and
517 dedifferentiated hepatocellular carcinoma cells revealed its implication in cell differentiation⁷².
518 Silencing of HDAC9 also suppressed adipogenic differentiation of preadipocytes⁷³.

519 Besides HDAC9, we found that the translation of PRDM12, a member of PRDM protein family,
520 recently implicated in pluripotency, was also upregulated by 5-FU. PRDM12 lacking the histone
521 lysine methyl-transferase intrinsic activity recruits G9a protein (encoded by EHMT2) to
522 dimethylate histone H3 on lysine 9 (H3K9me2) in embryonic carcinoma P19 cells⁷⁴, G9a being
523 essential for the maintenance of CRC stem cells^{75, 76}.

524

525 We also observed a translational decrease of three human AT-rich interaction domain (ARID)
526 family members ARID2, ARID1A, and ARID1B, which belong to the human SWI/SNF complex.
527 Downregulation and/or mutations in these ERGs are frequent in cancer⁷⁷ and have been
528 associated with pluripotency, cancer cell plasticity, cancer aggressivity and metastasis^{37, 78}.

529

530 Altogether, our data highlight the role of the 5-FU-driven modification of epigenetic regulation
531 in the emergence of the persister phenotype. In particular, translational changes of several
532 ERGs, occurring during and more strikingly after 5-FU treatment, are part of the molecular
533 mechanism sustaining cell plasticity, leading to a shift in cell identity and finally to the
534 acquisition of pluripotent and/or stemness features of persister cells.

535

536 Our translome analysis of genes coding for proteins involved in apoptosis revealed that a
537 strong pro-apoptotic signature occurred during 5-FU treatment, which was maintained
538 upregulated after 5-FU withdrawal. However, two survival proteins, TRAIL-R3, a decoy

539 receptor of the death receptor family, and BIRC3 (also known as cIAP2), a member of the anti-
540 apoptotic family, were translationally upregulated. Therefore, by alleviating the 5-FU-induced
541 cell-death program, TRAIL-R3 and BIRC3 may explain, at least in part, why a significant
542 percentage of cells escaped 5-FU toxicity. This agrees with a recent study showing that
543 exposure to 5-FU activates NF- κ B and upregulates BIRC3 in CRC cells, leading to the
544 promotion of anastasis, a cellular process through which cells survive the activation of
545 executioner caspases under stress ⁷⁹. Likewise, concurrent high expression of TRAIL-R3 and
546 low expression of TRAIL-R1 in primary CRC have previously been linked to a poor response
547 to first-line chemotherapy based on 5-FU, mirroring to the translational expression pattern
548 observed at D7 in this study ⁸⁰. In parallel, by examining translation of genes encoding proteins
549 involved in the cell cycle, we discovered 5-FU induces an early and continuous increase in the
550 translation of *CDKN1A* encoding P21, a pivotal inhibitor of cell cycle progression ⁸¹ whatever
551 the p53 mutated status.

552
553 Here, we also demonstrate that 5-FU steered cells towards senescence and we performed a
554 detailed analysis of the translationally deregulated genes implicated in SASP, to uncover their
555 temporal expression pattern, unveiling a potential deleterious effect for patient outcome.
556 Indeed, we discovered that most SASP markers are subjected to a strong upregulation of their
557 translational efficiency during treatment. Another set of SASP-associated genes, including
558 *NRG1* growth factor and *CXCL1*, *CXCL3*, and *CXCL8* cytokines, also showed increased
559 translation in persister cells. By interacting with integrins and subsequently with ERBB3, NRG1
560 activates pro-proliferative MAPK signaling, that sustains persister cells ⁸². Here, the
561 translational increase of NRG1 mRNA by 5-FU was accompanied by a similar increase in
562 cytoplasmic NRG1 mRNA, indicative of a buffered translational regulation. In contrast, the
563 expression of *CXCL1*, *CXCL3*, and *CXCL8* cytokines was essentially controlled at the
564 translational level through an active translational mechanism. Therefore, our study, by
565 pointing out a disconnection between the amount of stable cytoplasmic mRNA (reflecting
566 transcriptional and post-transcriptional control) and the translational activity, unraveled for the
567 first time that translation takes control and acts as compensatory mechanism allowing
568 synthesis of these cytokines through the 5-FU dependent inhibition of their transcriptional and
569 post-transcriptional control.

570
571 Our findings could have major impacts for the long-term management of the cancer disease
572 since, this production of several SASP factors involving a translational regulation could be
573 deleterious for 5-FU-treated patient outcome. Several SASP factors have pro-tumoral
574 properties by stimulating stemness, proliferation, migration and invasion, angiogenesis, and
575 immune evasion ⁸³. They can affect surrounding cells and ultimately promote cancer
576 progression, and contribute to disease recurrence. Among SASP factors, IL-6 and IL-8, two
577 abundant pro-inflammatory cytokines, drive most of the deleterious effects of SASP ⁸⁴.

578
579 So far, most senescent signatures relied on transcriptomic data ^{85, 86}. While a proteomic atlas
580 of senescence-associated secretome was recently proposed for aging ⁸⁷, recent
581 recommendations to detect senescent cells, either in normal or cancer context, still relied on
582 transcriptomic biomarkers ^{45, 88}. Here we provide strong evidence that considering translation
583 can reveal the expression of SASP factors, which would have gone unnoticed by analyzing the
584 transcriptome only.

585

586 For example, gaining insights in translome signatures of SASP-associated genes unveiled
587 that CXCL8 expression, that codes for a cytokine IL-8 playing a major role in cancer outcome,
588 was controlled at the translational level by 5-FU, and it increased far beyond treatment. Indeed,
589 IL-8 is a major pro-inflammatory and pro-tumoral cytokine^{50, 51, 89} whose expression regulation
590 is described at the transcriptional level, including its activation by NF- κ B and JNK pathways,
591 and at the post-translational level through a series of modifications, including glycosylation,
592 nitration and citrullination^{90, 91}. However, IL-8 has not previously been shown to be controlled
593 at the translational level. IL-8 binds to CXCR1 and CXCR2 receptors to attract neutrophils to
594 sites of injury and inflammation⁹⁰. Within the context of cancers, IL-8 facilitates cell
595 proliferation, migration and invasion⁹². In many cancers IL-8 impacts the microenvironment
596 through proangiogenic effect⁹³. It is considered as an inducer of immunosuppressive
597 microenvironment that, *in fine*, becomes pro-tumoral. This effect mainly resides on the capacity
598 of IL-8 to recruit to the tumor microenvironment, myeloid derived suppressor cells (MDSC),
599 which are highly immunosuppressive cells⁹⁴. Clinically, elevated levels of CXCL8 mRNA and
600 IL-8 protein are associated with a poorer prognosis in numerous cancers including CRC⁹⁵⁻⁹⁸.
601 In addition, *in cellulo* experiments showed that CXCL8 contributes to the development of
602 resistance to anti-cancer therapies⁸⁹, and targeting CXCL8 could overcome this resistance.
603 Emerging research utilizing *in vivo* models and clinical trials suggests the potential of targeting
604 CXCL8, in combination with standard anti-tumor therapies, such as chemotherapy, to enhance
605 outcomes in various cancers⁹⁰. Very recently, the NCT04599140 Phase I/II trial of the IL-8
606 receptor, CXCR1/2, antagonist SX-682, in combination with the anti-PDL1 Nivolumab, has
607 been initiated for RAS-mutated metastatic CRC⁹⁰.

608
609 Furthermore, we confirmed the interplay between HDAC9 and IL-8⁹⁹, by showing that silencing
610 HDAC9 decreased the 5-FU-driven overexpression of IL-8 (data not shown). Therefore, the
611 observation that HDAC9, whose translation is upregulated by 5-FU, could contribute to the 5-
612 FU-driven overexpression of IL-8, further strengthens the conclusion that 5-FU-driven
613 translational upregulation of key genes plays a major role in the drug's effects.
614 Our findings that IL-8 synthesis is stimulated by 5-FU and that targeting IL-8 is lethal for
615 persister cells reinforce the promising efforts being made to target this pathway to provide
616 clinical benefits in CRC when combined with a 5-FU based regimen.

617
618 In this study, through its stable integration within ribosomal RNA, we identified 5-FU as an
619 unsuspected master epi-transcriptomic driver of translational control. Recent reviews have
620 highlighted emerging hallmarks of cancer, including senescence, cell plasticity, and epigenetic
621 reprogramming, all interconnected with tumor-promoting inflammation¹⁰⁰. Here we unraveled
622 that a translational reprogramming, induced by exogeneous addition of 5-FU, impacts genes
623 representing each of these hallmarks. In sum, 5-FU sustains the translation of a panel of
624 mRNAs encoding anti-apoptotic factors, epigenetic regulators, pro-inflammatory cytokines with
625 pro-tumoral activities driving the emergence of persister cells, allowing them to escape the
626 DNA mediated cytotoxic effects of 5-FU and ultimately to promote tumor progression and
627 resistance.

628 **Material and Methods**

629

630 ***Cell lines, cell culture, and 5-FU treatment***

631 The CRC cell lines, HCT-116 (ATCC CCL-247) and HT-29 (ATCC HTB-38), were obtained
632 from ATCC. These cell lines were authenticated by PCRsingle-locus-technology (Eurofins,
633 Ebersberg, Germany). CRC cells were maintained in Dulbecco Minimum Essential Medium—
634 GlutaMax (Invitrogen) supplemented with 10% fetal bovine serum (FBS), penicillin (100U/mL)
635 and streptomycin (100µg/mL) at 37 °C with 5% CO₂. Cells were routinely tested against
636 mycoplasma infection. Cells were plated 48 h before 5-FU treatment. 5-FU was kindly provided
637 by the Centre Léon Bérard (Lyon, FRANCE). The stock solution (ACCORD 50mg/ml) was
638 diluted immediately before use in DMEM and added to cell culture medium.

639

640 ***Cell Infections***

641 CRC cells were infected using Human Nanog pGreenZeo Differentiation Reporter (System
642 Biosciences SR10030VA-1) (www.systembio.com) according to the manufacturer's protocol.
643 Nanog pGreenZeo-infected cells were "colored" using rLV.EF1.AmCyan (Flash therapeutics
644 0011VCT/0039VCT) or rLV.EF1.mCherry-9 (Flash therapeutics 0011VCT/0039VCT)
645 according to the manufacturer's protocol. Cells were sorted by FACS (Fluorescence Activated
646 Cell Sorting) on the FACS ARIA IIU BECTON DICKINSON to get a homogenous red or blue
647 cell population. Data were analyzed with FlowJo Software.

648

649 ***Immunofluorescence***

650 CRC cells were seeded on slides and then fixed using buffered 10% formalin for 10 min. The
651 permeabilization step was performed for 10 min at room temperature (RT) with TBS containing
652 0.5% Triton X-100. Non-specific binding sites were blocked with blocking buffer (TBS, 5%
653 Donkey serum, 0.2% Triton X-100). Incubation with primary antibodies (NANOG ab21624,
654 GFP GFP-1010) was performed overnight at 4°C. The next day, slides were washed and then
655 incubated with secondary antibodies at RT for 1 hour. Fluorescent secondary antibodies
656 (Donkey Fluor488 anti-mouse or donkey 647 anti-rabbit from Jackson Immuno Research) were
657 added for 1 h and nuclei were stained with DAPI. Slides were mounted using fluoromount G
658 and then observed under an epifluorescent microscope (Zeiss AxioImager Z1).

659

660 ***ELISA***

661 Supernatants were collected after two days of incubation and then centrifuged for 10 minutes
662 at 2,000g. Cells were then trypsinized and quantified. Samples were aliquoted and stored at -
663 80°C. ELISA for CXCL1 (Peprotech® 900-M83), CXCL8 (Peprotech® 900-M18), and CXCL3
664 (Abcam ab234574) was performed according to the manufacturer's ELISA Sandwich protocol.
665 Briefly, the plate is pre-coated with capture antibody, then samples and finally the detection
666 antibody are added. Following the addition of the detection antibody, a chemical substrate is
667 added to produce a colorimetric signal that can be read by an ELISA plate reader at
668 absorbance of 405nm. All obtained concentrations were normalized for 10⁶ cells.

669

670 ***SiRNA design and transfection of cells***

671 SiRNA were designed using siRNA design websites
672 (<https://rnaidesigner.thermofisher.com/rnaiexpress/>) and
673 (<https://eurofinsgenomics.eu/en/ecom/tools/sirna-design/>) and were synthesized by
674 Eurogentec ([Extended Data Table 4](#)). Briefly, CRC cells were transfected for 48h hours
675 according to the Invitrogen Lipofectamine RNAiMAX protocol with siRNA at a 20pM final

676 concentration
677 ([https://assets.thermofisher.com/TFSAssets/LSG/manuals/Lipofectamine_RNAiMAX_Reag_](https://assets.thermofisher.com/TFSAssets/LSG/manuals/Lipofectamine_RNAiMAX_Reag_protocol.pdf)
678 [protocol.pdf](https://assets.thermofisher.com/TFSAssets/LSG/manuals/Lipofectamine_RNAiMAX_Reag_protocol.pdf)).

679

680 ***RNA extraction and RT-qPCR***

681 Total RNA was extracted using the RNeasy Mini Kit (Qiagen) according to the manufacturer's
682 instructions. For RT-qPCR analyses, cDNA was synthesized using SuperScript II and random
683 hexamer (both from Invitrogen). Quantitative gene expression was performed using SYBR
684 Green master mix on a LightCycler 480 Instrument (both from Roche). Results were
685 normalized to GAPDH expression and analyzed using the $\Delta\Delta C_t$ method. Primer sequences
686 are listed in [Extended Data Table 4](#).

687

688 ***Western blotting***

689 CRC cells were harvested and lysed in Laemmli buffer (0.5M Tris-HCL, 10% SDS, 10%
690 Glycerol and 0.1M DTT). Forty micrograms of total protein lysates were run on a 4-20% SDS
691 polyacrylamide gel and transferred onto a nitrocellulose membrane. The membrane was
692 blocked with 5% nonfat milk in TBS-Tween (TBST). The primary antibodies (listed in [Extended](#)
693 [Data Table 4](#)) were incubated overnight at 4°C in 3% milk-TBST or BSA-TBST. Proteins were
694 detected by chemiluminescence with an anti-rabbit or anti-mouse HRP-conjugated antibody
695 and ECL substrate (Covalab (Bron France). Images were collected on a ChemiDoc XRS+ (Bio-
696 Rad (Hercules, CA, USA), and the signal was analyzed with Bio-Rad ImageLab software.

697

698 ***5-FU analysis by Liquid Chromatography-High Resolution Mass Spectrometry (LC- 699 HRMS)***

700 RNAs were extracted from 150 μ L of each of the fractions using TRIzol™ LS reagent
701 (Invitrogen) following manufacturer's instructions and suspended in RNase-free water. RNA
702 extracted from specific polysome fractions were loaded on a 1% low-melting point agarose gel
703 (Life Technologies). After electrophoretic separation of RNA samples, the 28S and 18S bands
704 were cut from the gel and RNA was extracted from agarose using Nucleospin Gel and PCR
705 clean-up (Macherey-Nagel) columns.

706 Purified rRNA (1 to 3 μ g) was digested overnight at 37 °C with 270 units of Nuclease S1
707 (Promega) using the supplied buffer. Next, nucleotides were dephosphorylated, by directly
708 adding 5U of calf intestine phosphatase to the mix (New England Biolabs) in 100 mM Tris-HCl,
709 50 mM NaCl, 10 mM MgCl₂, 0.025% Triton® X-100. Digestion was carried out overnight at 37
710 °C and the digested mix was then stored at -80 °C. Before LC-HRMS analysis, 300 μ L of a
711 mixture methanol/water (70/30, v/v) and labelled internal standards were added to samples.
712 After homogenization and centrifugation, the supernatants were transferred into tubes to be
713 evaporated to dryness under nitrogen. Then, the dry residues were resuspended in 100 μ L of
714 water before injection of a volume of 10 μ L into the LC-HRMS device. The device was
715 constituted with Ultimate 3000 modules and a Q Exactive Plus mass spectrometer (Thermo
716 Scientific). Analysis were performed according to the previously published method ¹⁰¹.

717 The level of 5-FU per ribosome was calculated as the ratio of measured [5-FUrd] over the
718 measured [A], [C] and [G], divided by the relative quantity of each nucleotide per ribosome.

719

720 ***Polysome profiling***

721 CRC cells were seeded at 10⁶ cells/10cm dish. Forty-eight hours after seeding, HCT-116 were
722 treated with 10 μ M 5-FU over 48h. At each time point of the experiment (namely D0 (before
723 adding 5-FU to medium), D1, D2 and D7), cells were treated for 10 min with emetin (Sigma)

724 25µg/ml, washed twice with PBS, and harvested by trypsination. Cytoplasmic lysates were
725 prepared by incubation of cells for 10 min in hypotonic buffer (10 mM Tris-HCl pH 7.4, 0.5 mM
726 MgCl₂, 10 mM KCl, 1X Complete™ EDTA free protease inhibitor (Roche) and 10 U/mL
727 RNaseOut™ (Invitrogen)) followed by addition of 0.7 % NP-40. Swelling cells are lysed by
728 shaking in Precellys Evolution tissue homogenizer (10s, 4500rpm). Nuclei were pelleted by
729 centrifugation at 750 g for 5 min at 4°C, and mitochondria were pelleted by centrifugation at
730 12,000 g for 10 min at 4°C. The protein content of the cytosolic extract was measured by
731 Bradford assay and samples containing 2mg protein were loaded over 15–50% sucrose
732 gradients (poured using the Gradient Master (Serlabo Technologies). After ultracentrifugation
733 at 38,000rpm for 105 min at 4°C on a SW41 Beckman rotor, 18 fractions of 700µl each were
734 collected from each gradient while 254nm absorbance profiles were generated using an ISCO
735 UA-6 detector. RNA samples were extracted from 150 µL of each polysomal fraction using
736 TRIzol™ LS reagent (Invitrogen) following manufacturer's instructions and suspended in
737 RNase-free water. A fraction of each sample was loaded on an agarose gel, to identify their
738 RNA content, and polysomal fractions containing mRNA with more than three ribosomes were
739 pooled.

740

741 ***Translatome analysis***

742 RNA-seq libraries were prepared using the Universal Plus mRNA-seq kit (Tecan Trading AG,
743 Switzerland) according to the manufacturer's instructions. Briefly, polyadenylated RNAs were
744 selected using oligo-dT magnetic beads. We fragmented the polyA+ RNAs using divalent
745 cations at elevated temperature and reverse-transcribed them using random hexamers,
746 reverse transcriptase and actinomycin D. Deoxy-TTP was replaced by dUTP during the second
747 strand synthesis to prevent its amplification by PCR. We repaired the double-stranded cDNAs
748 and we adenylated them at their 3' ends followed by a ligation to Tecan adaptors including
749 UDIs. We submitted ligated cDNAs to a strand selection prior to a PCR amplification for 15
750 cycles and purified the PCR products using AMPure XP Beads (Beckman Coulter Genomics,
751 Brea, CA, USA). The size distribution of the resulting libraries was monitored using a Fragment
752 Analyzer (Agilent Technologies, Santa Clara, CA, USA) and the libraries were quantified using
753 the KAPA Library quantification kit (Roche, Basel, Switzerland).

754 Libraries were denatured with NaOH, neutralized with Tris-HCl, and diluted to 300 pM. We
755 performed the clustering and sequencing on a NovaSeq 6000 (Illumina, San Diego, CA, USA)
756 using the single-read 100nt protocol on an S2 flow cell, to generate 50 to 84 million sequences.

757

758 ***Bioinformatic analysis of translomic data***

759 Transcriptome (cytosomal fraction) and translatome (polysomal fraction) libraries read quality
760 were assessed using FastQC v0.11.9 (Babraham Institute, Cambridge, UK). Reads were
761 filtered according to quality threshold Q35, and were trimmed of 10 bases at their start, using
762 Cutadapt v3.2¹⁰². With Cutadapt, we set the minimal length of trimmed reads at 50 nucleotides;
763 all trimmed reads shorter than 50 were removed from the analysis. High quality reads were
764 then aligned using STAR v2.7.9a¹⁰³, on the release 104 of the Homo sapiens reference
765 genome GRCh38 primary_assembly, and annotated with the GRCh38.104 Ensembl
766 annotation file. Quantification of mapped reads was performed using featureCounts from
767 subread v2.0.1¹⁰⁴.

768 Statistical differential analyses were performed between the different times of the kinetic. Day
769 0 (D0) was used as control and compared to others times of the kinetic (D1, D2 and D7) for
770 each fraction, whether cytoplasmic and polysomal (> at 3 ribosomes on the RNA). Statistics
771 used Wald test from DESeq2 R package v1.30.1¹⁰⁵ (Supplementary Tables 1, 2 and 3).

772 For each dataset, the read counts were filtered with a minimum of 1 count per million per
773 biological sample after size factors estimation (Relative Log Expression normalization), and
774 then dispersion was estimated (using DESeq2). P-value adjustment that corrects for multiple
775 tests to lower the risk of false discovery was performed with the method of Benjamini and
776 Hochberg¹⁰⁶. Genes with BH corrected p-values below 0.05 were kept. Then, results from
777 these simple comparisons are used in a double comparison between fractions to categorize
778 genes involved in transcription or translation or in both mechanisms, using Pandas v1.1.5¹⁰⁷.
779 Gene identifications were performed with biobnet dbtodb API¹⁰⁸. Functional annotations were
780 performed with gProfileR v0.2.1¹⁰⁹ using a g:SCS threshold < at 0.05. GO terms were then
781 classified according to their depths and levels using goatools v1.3.1¹¹⁰. Differential transcripts
782 were annotated from the databases with msigdb R package v1.2.0¹¹¹. Fisher p-value corrected
783 by FDR were performed on results from the enrichment according to the probability of their
784 presence in the human genome. The heatmap was performed using matplotlib v3.3.0, seaborn
785 v0.11.2, pandas v1.1.5 and clustergrammer v2^{107, 112-114}. PCA in 3 dimensions was performed
786 with rgl R package¹¹⁵.

787 The list of differentially translated Epigenetic regulator genes (Fig. 3b,c) was generated using
788 a cut off p-adj < 0.05. The intersection of deregulated ERGs at different time points was
789 generated using <https://bioinformatics.psb.ugent.be/webtools/Venn/>.

790 For the GSEA analysis, gene lists and corresponding adjusted p-values and log2 Fold Change
791 were taken from the translatoome analysis of the polysomal fraction. Genes were ranked from
792 the most significantly upregulated to most significantly downregulated and a pre-ranked GSEA
793 analysis was performed using the GSEA software (version 4.3.2) downloaded from
794 <https://www.gsea-msigdb.org>, using several gene sets (Hallmarks :
795 h.all.v2023.1.Hs.symbols.gmt, C2 subcollections including C2 CPG : Chemical and Genetic
796 perturbation c2.cgp.v2023.1.Hs.symbols.gmt and KEGG database
797 c2.cp.kegg.v2023.1.Hs.symbols.gmt, C5 : GO Term Biological Process
798 c5.go.bp.v2023.1.Hs.symbols.gmt).

799

800 ***Flow cytometry for apoptosis and cell cycle analysis***

801 One to two million CRC cells were harvested at different time point after 5-FU treatment (D0,
802 D2, D5 and D7). For the apoptosis assay, the cells were processed according to the FITC
803 active caspase 3 apoptosis kit procedure (BD PharmingenTM, reference 550480). After staining
804 with the FITC active caspase 3 antibody, the cells were incubated with FxCycleTM Violet Stain
805 accordingly to the manufacturer's instructions. FITC and FxCycleTM Violet Stain fluorescence
806 was monitored by Flow cytometer (BD LSRFortessaTM Cell Analyzer) and the results were
807 analyzed using FlowJoTM v10.9.0 Software (BD Life Sciences). For the cell cycle assay, CRC
808 cells were trypsinized, collected and stabilized *via* 70% ethanol at 20°C. After rinsing twice with
809 cold PBS, CRC cells were stained with 500 µL Propidium Iodide (PI, Sigma-Aldrich) and
810 incubated for 30 min at room temperature. Cell cycle assessment was performed using a BD
811 FACSCanto II flow cytometer and the results were analyzed using FlowJoTM v10.9.0 Software
812 (BD Life Sciences). One-way ANOVA followed by Dunnett's multiple comparisons testing was
813 performed using GraphPad Prism version 10.0.0 for Windows, GraphPad Software, Boston,
814 Massachusetts USA, www.graphpad.com.

815

816 ***SA-beta-Gal assay***

817 CRC cells were washed once with PBS 1X and fixed for 5 min in fixation solution containing
818 2% formaldehyde and 0.2% glutaraldehyde. They were then rinsed twice with PBS 1X and
819 incubated overnight at 37°C in SA-β-galactosidase staining solution containing 40 mM citric

820 acid/sodium phosphate buffer pH 6, 5 mM K₃[Fe(CN)₆], 5 mM K₄[Fe(CN)₆] 3H₂O, 150 mM
821 sodium chloride, 2 mM magnesium chloride and 1 mg/mL X-gal, as described in Dimri *et al*⁴¹.
822 At least 100 cells were counted for each condition.

823

824 **Cancer stem cell frequency**

825 Following 5FU treatment, viable cells, selected by a viability marker (Sytox Blue), were sorted
826 using the Becton Dickinson cytometer Melody. Alive CRC cells were plated in 96-well plates
827 under low adhesion conditions (plate coated with polyhema) in M11 medium, at different
828 densities (1, 10, 100, or 1000 cells/well). The M11 medium composition was as follows: DMEM
829 F12 glutaMAX (ref 31331-028), EGF (MACS, ref 130-097-751) (20ng/ml), FGF-2 (MACS, ref
830 130-093-564) (10ng/ml), insulin (Sigma, ref I9278) (0.02mg/ml), N2 100X (ref 17502-048),
831 streptomycin-penicillin 100X (100U/ml-100µg/ml), glucose 30% (0.3%). Number of spheres
832 was determined after 4-7 days of incubation. Cancer Stem Cell frequency was evaluated using
833 the software: <https://bioinf.wehi.edu.au/software/elda/>¹¹⁶.

834

835 **Viability assay**

836 Cell viability was assessed using the Trypan blue-exclusion test. Briefly, along the 5-FU
837 kinetics, CRC cells were trypsinized and collected. Ten microliters of trypan blue (Invitrogen)
838 were added to 10µL of cellular suspension. Cells were counted at the indicated time (Ozyme
839 counter). For siRNA experiments, 70,000 cells/well were seeded in 24-well plates. Cells were
840 co-treated for 48h as follows: 5-FU (10µM) + reparixin 1nM or 5-FU (10µM) + siCXCL8 20pM
841 or 5-FU (10µM) + siCTRL 20pM. Reparixin was administrated every 2 days, while siRNA was
842 administrated on D0, D7 and D12 for two days. Cells were trypsinized and counted at the
843 indicated times.

844

845 **In vivo experiments**

846 A million cells (HCT-116 hNanog or HT-29 hNanog) were injected subcutaneously into the
847 right flanks on NOD/SCID mice (Charles River) in a 1:1 mixture of Matrigel and PBS in a final
848 volume of 100 µL. Tumor apparition and volume ($[\text{length} \times \text{width}^2]/2$) were measured.

849

850 **References**

851

- 852 1. Longley, D.B., Harkin, D.P. & Johnston, P.G. 5-fluorouracil: mechanisms of action and
853 clinical strategies. *Nat Rev Cancer* **3**, 330-338 (2003).
- 854 2. Gmeiner, W.H. & Okechukwu, C.C. Review of 5-FU resistance mechanisms in
855 colorectal cancer: clinical significance of attenuated on-target effects. *Cancer Drug*
856 *Resist* **6**, 257-272 (2023).
- 857 3. Bray, F. *et al.* Global cancer statistics 2018: GLOBOCAN estimates of incidence and
858 mortality worldwide for 36 cancers in 185 countries. *CA: a cancer journal for clinicians*
859 **68**, 394-424 (2018).
- 860 4. Sargent, D. *et al.* Evidence for cure by adjuvant therapy in colon cancer: observations
861 based on individual patient data from 20,898 patients on 18 randomized trials. *J Clin*
862 *Oncol* **27**, 872-877 (2009).
- 863 5. Shen, S., Vagner, S. & Robert, C. Persistent Cancer Cells: The Deadly Survivors. *Cell*
864 **183**, 860-874 (2020).
- 865 6. Phan, T.G. & Croucher, P.I. The dormant cancer cell life cycle. *Nat Rev Cancer* **20**,
866 398-411 (2020).
- 867 7. Marine, J.C., Dawson, S.J. & Dawson, M.A. Non-genetic mechanisms of therapeutic
868 resistance in cancer. *Nat Rev Cancer* **20**, 743-756 (2020).
- 869 8. Kunz, C. *et al.* Base excision by thymine DNA glycosylase mediates DNA-directed
870 cytotoxicity of 5-fluorouracil. *PLoS Biol* **7**, e91 (2009).
- 871 9. Fischer, F., Baerenfaller, K. & Jiricny, J. 5-Fluorouracil is efficiently removed from DNA
872 by the base excision and mismatch repair systems. *Gastroenterology* **133**, 1858-1868
873 (2007).
- 874 10. Lonn, U. & Lonn, S. DNA lesions in human neoplastic cells and cytotoxicity of 5-
875 fluoropyrimidines. *Cancer Res* **46**, 3866-3870 (1986).
- 876 11. Parker, W.B., Kennedy, K.A. & Klubes, P. Dissociation of 5-fluorouracil-induced DNA
877 fragmentation from either its incorporation into DNA or its cytotoxicity in murine T-
878 lymphoma (S-49) cells. *Cancer Res* **47**, 979-982 (1987).
- 879 12. Wyatt, M.D. & Wilson, D.M., 3rd Participation of DNA repair in the response to 5-
880 fluorouracil. *Cell Mol Life Sci* **66**, 788-799 (2009).
- 881 13. Chalabi-Dchar, M. *et al.* A novel view on an old drug, 5-fluorouracil: an unexpected
882 RNA modifier with intriguing impact on cancer cell fate. *NAR Cancer* **3**, zcab032 (2021).
- 883 14. Pettersen, H.S. *et al.* UNG-initiated base excision repair is the major repair route for 5-
884 fluorouracil in DNA, but 5-fluorouracil cytotoxicity depends mainly on RNA
885 incorporation. *Nucleic Acids Res* **39**, 8430-8444 (2011).
- 886 15. Pritchard, D.M., Watson, A.J., Potten, C.S., Jackman, A.L. & Hickman, J.A. Inhibition
887 by uridine but not thymidine of p53-dependent intestinal apoptosis initiated by 5-
888 fluorouracil: evidence for the involvement of RNA perturbation. *Proc Natl Acad Sci U S*
889 *A* **94**, 1795-1799 (1997).
- 890 16. Takimoto, C.H., Tan, Y.Y., Cadman, E.C. & Armstrong, R.D. Correlation between
891 ribosomal RNA production and RNA-directed fluoropyrimidine cytotoxicity. *Biochemical*
892 *pharmacology* **36**, 3243-3248 (1987).
- 893 17. Burger, K. *et al.* Chemotherapeutic drugs inhibit ribosome biogenesis at various levels.
894 *J Biol Chem* **285**, 12416-12425 (2010).
- 895 18. Therizols, G. *et al.* Alteration of ribosome function upon 5-fluorouracil treatment favors
896 cancer cell drug-tolerance. *Nat Commun* **13**, 173 (2022).
- 897 19. Maxwell, P.J. *et al.* Identification of 5-fluorouracil-inducible target genes using cDNA
898 microarray profiling. *Cancer Res* **63**, 4602-4606 (2003).
- 899 20. Mariadason, J.M., Arango, D. & Augenlicht, L.H. Customizing chemotherapy for colon
900 cancer: the potential of gene expression profiling. *Drug Resist Updat* **7**, 209-218 (2004).
- 901 21. Zhang, W. *et al.* Apoptotic response to 5-fluorouracil treatment is mediated by reduced
902 polyamines, non-autocrine Fas ligand and induced tumor necrosis factor receptor 2.
903 *Cancer Biol Ther* **2**, 572-578 (2003).

- 904 22. Laroche-Clary, A. *et al.* Absence of transcriptomic signature of response to
905 chemotherapy in metastatic colorectal carcinoma patients. *Pharmacogenomics* **13**,
906 497-504 (2012).
- 907 23. Rodrigues, D. *et al.* Drug-induced gene expression profile changes in relation to
908 intestinal toxicity: State-of-the-art and new approaches. *Cancer Treat Rev* **77**, 57-66
909 (2019).
- 910 24. Park, S.R. *et al.* Single-Cell Transcriptome Analysis of Colon Cancer Cell Response to
911 5-Fluorouracil-Induced DNA Damage. *Cell Rep* **32**, 108077 (2020).
- 912 25. Ge, J., Karijolich, J., Zhai, Y., Zheng, J. & Yu, Y.T. 5-Fluorouracil Treatment Alters the
913 Efficiency of Translational Recoding. *Genes (Basel)* **8** (2017).
- 914 26. Marin-Vicente, C., Lyutvinskiy, Y., Romans Fuertes, P., Zubarev, R.A. & Visa, N. The
915 effects of 5-fluorouracil on the proteome of colon cancer cells. *J Proteome Res* **12**,
916 1969-1979 (2013).
- 917 27. Liu, Z. *et al.* Quantitative proteomic and phosphoproteomic studies reveal novel 5-
918 fluorouracil resistant targets in hepatocellular carcinoma. *J Proteomics* **208**, 103501
919 (2019).
- 920 28. Sun, R. *et al.* Proteomic Analysis Reveals that EPHX1 Contributes to 5-Fluorouracil
921 Resistance in a Human Hepatocellular Carcinoma Cell Line. *Proteomics Clin Appl* **14**,
922 e1900080 (2020).
- 923 29. Casale, F. *et al.* Plasma concentrations of 5-fluorouracil and its metabolites in colon
924 cancer patients. *Pharmacological research* **50**, 173-179 (2004).
- 925 30. Trump, D.L. *et al.* Pharmacokinetic and pharmacodynamic analysis of fluorouracil
926 during 72-hour continuous infusion with and without dipyridamole. *J Clin Oncol* **9**, 2027-
927 2035 (1991).
- 928 31. Green, D.R. & Kroemer, G. Cytoplasmic functions of the tumour suppressor p53.
929 *Nature* **458**, 1127-1130 (2009).
- 930 32. Wang, J., Levasseur, D.N. & Orkin, S.H. Requirement of Nanog dimerization for stem
931 cell self-renewal and pluripotency. *Proc Natl Acad Sci U S A* **105**, 6326-6331 (2008).
- 932 33. Hepburn, A.C. *et al.* The induction of core pluripotency master regulators in cancers
933 defines poor clinical outcomes and treatment resistance. *Oncogene* **38**, 4412-4424
934 (2019).
- 935 34. Palla, A.R. *et al.* The pluripotency factor NANOG promotes the formation of squamous
936 cell carcinomas. *Sci Rep* **5**, 10205 (2015).
- 937 35. Bash-Imam, Z. *et al.* Translational reprogramming of colorectal cancer cells induced by
938 5-fluorouracil through a miRNA-dependent mechanism. *Oncotarget* **8**, 46219-46233
939 (2017).
- 940 36. Yadav, T., Quivy, J.P. & Almouzni, G. Chromatin plasticity: A versatile landscape that
941 underlies cell fate and identity. *Science* **361**, 1332-1336 (2018).
- 942 37. Wainwright, E.N. & Scaffidi, P. Epigenetics and Cancer Stem Cells: Unleashing,
943 Hijacking, and Restricting Cellular Plasticity. *Trends Cancer* **3**, 372-386 (2017).
- 944 38. Halaburkova, A. *et al.* Pan-cancer multi-omics analysis and orthogonal experimental
945 assessment of epigenetic driver genes. *Genome Res* **30**, 1517-1532 (2020).
- 946 39. Ahmed, D. *et al.* Epigenetic and genetic features of 24 colon cancer cell lines.
947 *Oncogenesis* **2**, e71 (2013).
- 948 40. Campisi, J. & d'Adda di Fagagna, F. Cellular senescence: when bad things happen to
949 good cells. *Nat Rev Mol Cell Biol* **8**, 729-740 (2007).
- 950 41. Dimri, G.P. *et al.* A biomarker that identifies senescent human cells in culture and in
951 aging skin in vivo. *Proc Natl Acad Sci U S A* **92**, 9363-9367 (1995).
- 952 42. Collin, G., Huna, A., Warnier, M., Flaman, J.M. & Bernard, D. Transcriptional repression
953 of DNA repair genes is a hallmark and a cause of cellular senescence. *Cell Death Dis*
954 **9**, 259 (2018).
- 955 43. Freund, A., Laberge, R.M., Demaria, M. & Campisi, J. Lamin B1 loss is a senescence-
956 associated biomarker. *Mol Biol Cell* **23**, 2066-2075 (2012).

- 957 44. Coppe, J.P. *et al.* Senescence-associated secretory phenotypes reveal cell-
958 nonautonomous functions of oncogenic RAS and the p53 tumor suppressor. *PLoS Biol*
959 **6**, 2853-2868 (2008).
- 960 45. Gorgoulis, V. *et al.* Cellular Senescence: Defining a Path Forward. *Cell* **179**, 813-827
961 (2019).
- 962 46. Was, H. *et al.* Some chemotherapeutics-treated colon cancer cells display a specific
963 phenotype being a combination of stem-like and senescent cell features. *Cancer Biol*
964 *Ther* **19**, 63-75 (2018).
- 965 47. Arnandis, T. *et al.* Oxidative Stress in Cells with Extra Centrosomes Drives Non-Cell-
966 Autonomous Invasion. *Dev Cell* **47**, 409-424 e409 (2018).
- 967 48. Zhang, B. *et al.* The senescence-associated secretory phenotype is potentiated by
968 feedforward regulatory mechanisms involving Zscan4 and TAK1. *Nat Commun* **9**, 1723
969 (2018).
- 970 49. Kiss, Z., Mudryj, M. & Ghosh, P.M. Non-circadian aspects of BHLHE40 cellular function
971 in cancer. *Genes Cancer* **11**, 1-19 (2020).
- 972 50. Waugh, D.J. & Wilson, C. The interleukin-8 pathway in cancer. *Clin Cancer Res* **14**,
973 6735-6741 (2008).
- 974 51. Xiong, X. *et al.* CXCL8 in Tumor Biology and Its Implications for Clinical Translation.
975 *Front Mol Biosci* **9**, 723846 (2022).
- 976 52. Casasanta, M.A. *et al.* Fusobacterium nucleatum host-cell binding and invasion
977 induces IL-8 and CXCL1 secretion that drives colorectal cancer cell migration. *Sci*
978 *Signal* **13** (2020).
- 979 53. Rawla, P., Sunkara, T. & Gaduputi, V. Epidemiology of Pancreatic Cancer: Global
980 Trends, Etiology and Risk Factors. *World journal of oncology* **10**, 10-27 (2019).
- 981 54. Sung, H. *et al.* Global Cancer Statistics 2020: GLOBOCAN Estimates of Incidence and
982 Mortality Worldwide for 36 Cancers in 185 Countries. *CA: a cancer journal for clinicians*
983 **71**, 209-249 (2021).
- 984 55. Xi, Y., Nakajima, G., Schmitz, J.C., Chu, E. & Ju, J. Multi-level gene expression profiles
985 affected by thymidylate synthase and 5-fluorouracil in colon cancer. *BMC Genomics* **7**,
986 68 (2006).
- 987 56. Kudo, K. *et al.* Translational control analysis by translationally active RNA
988 capture/microarray analysis (TrIP-Chip). *Nucleic Acids Res* **38**, e104 (2010).
- 989 57. Houghton, J.A., Houghton, P.J. & Wooten, R.S. Mechanism of induction of
990 gastrointestinal toxicity in the mouse by 5-fluorouracil, 5-fluorouridine, and 5-fluoro-2'-
991 deoxyuridine. *Cancer Res* **39**, 2406-2413 (1979).
- 992 58. Kufe, D.W. & Major, P.P. 5-Fluorouracil incorporation into human breast carcinoma
993 RNA correlates with cytotoxicity. *J Biol Chem* **256**, 9802-9805 (1981).
- 994 59. Liang, Y.Y. *et al.* CETSA interaction proteomics define specific RNA-modification
995 pathways as key components of fluorouracil-based cancer drug cytotoxicity. *Cell Chem*
996 *Biol* **29**, 572-585 e578 (2022).
- 997 60. Kemper, K., de Goeje, P.L., Peeper, D.S. & van Amerongen, R. Phenotype switching:
998 tumor cell plasticity as a resistance mechanism and target for therapy. *Cancer Res* **74**,
999 5937-5941 (2014).
- 1000 61. Rambow, F. *et al.* Toward Minimal Residual Disease-Directed Therapy in Melanoma.
1001 *Cell* **174**, 843-855 e819 (2018).
- 1002 62. Boumahdi, S. & de Sauvage, F.J. The great escape: tumour cell plasticity in resistance
1003 to targeted therapy. *Nat Rev Drug Discov* **19**, 39-56 (2020).
- 1004 63. Nassar, D. & Blanpain, C. Cancer Stem Cells: Basic Concepts and Therapeutic
1005 Implications. *Annu Rev Pathol* **11**, 47-76 (2016).
- 1006 64. de Sousa, E.M.F. & de Sauvage, F.J. Cellular Plasticity in Intestinal Homeostasis and
1007 Disease. *Cell Stem Cell* **24**, 54-64 (2019).
- 1008 65. Wajapeyee, N. & Gupta, R. Epigenetic Alterations and Mechanisms That Drive
1009 Resistance to Targeted Cancer Therapies. *Cancer Res* **81**, 5589-5595 (2021).
- 1010 66. Rehman, S.K. *et al.* Colorectal Cancer Cells Enter a Diapause-like DTP State to
1011 Survive Chemotherapy. *Cell* **184**, 226-242 e221 (2021).

- 1012 67. Zhang, B., Lin, J., Zhang, J., Wang, X. & Deng, X. Integrated Chromatin Accessibility
1013 and Transcriptome Landscapes of 5-Fluorouracil-Resistant Colon Cancer Cells. *Front*
1014 *Cell Dev Biol* **10**, 838332 (2022).
- 1015 68. Brancolini, C., Gagliano, T. & Minisini, M. HDACs and the epigenetic plasticity of cancer
1016 cells: Target the complexity. *Pharmacol Ther* **238**, 108190 (2022).
- 1017 69. Gil, V.S. *et al.* Deregulated expression of HDAC9 in B cells promotes development of
1018 lymphoproliferative disease and lymphoma in mice. *Dis Model Mech* **9**, 1483-1495
1019 (2016).
- 1020 70. Xu, L. *et al.* HDAC9 Contributes to Serous Ovarian Cancer Progression through
1021 Regulating Epithelial-Mesenchymal Transition. *Biomedicines* **10** (2022).
- 1022 71. Xiong, K., Zhang, H., Du, Y., Tian, J. & Ding, S. Identification of HDAC9 as a viable
1023 therapeutic target for the treatment of gastric cancer. *Exp Mol Med* **51**, 1-15 (2019).
- 1024 72. Kanki, K., Watanabe, R., Nguyen Thai, L., Zhao, C.H. & Naito, K. HDAC9 Is
1025 Preferentially Expressed in Dedifferentiated Hepatocellular Carcinoma Cells and Is
1026 Involved in an Anchorage-Independent Growth. *Cancers (Basel)* **12** (2020).
- 1027 73. Chatterjee, T.K. *et al.* Histone deacetylase 9 is a negative regulator of adipogenic
1028 differentiation. *J Biol Chem* **286**, 27836-27847 (2011).
- 1029 74. Yang, C.M. & Shinkai, Y. Prdm12 is induced by retinoic acid and exhibits anti-
1030 proliferative properties through the cell cycle modulation of P19 embryonic carcinoma
1031 cells. *Cell Struct Funct* **38**, 197-206 (2013).
- 1032 75. Luo, C.W. *et al.* G9a governs colon cancer stem cell phenotype and
1033 chemoradioresistance through PP2A-RPA axis-mediated DNA damage response.
1034 *Radiother Oncol* **124**, 395-402 (2017).
- 1035 76. Bergin, C.J. *et al.* G9a controls pluripotent-like identity and tumor-initiating function in
1036 human colorectal cancer. *Oncogene* **40**, 1191-1202 (2021).
- 1037 77. Lin, C. *et al.* Recent advances in the ARID family: focusing on roles in human cancer.
1038 *OncoTargets and therapy* **7**, 315-324 (2014).
- 1039 78. Pagliaroli, L. & Trizzino, M. The Evolutionary Conserved SWI/SNF Subunits ARID1A
1040 and ARID1B Are Key Modulators of Pluripotency and Cell-Fate Determination. *Front*
1041 *Cell Dev Biol* **9**, 643361 (2021).
- 1042 79. Wang, R. *et al.* Anastasis enhances metastasis and chemoresistance of colorectal
1043 cancer cells through upregulating cIAP2/NFkappaB signaling. *Cell Death Dis* **14**, 388
1044 (2023).
- 1045 80. Granci, V. *et al.* Prognostic significance of TRAIL-R1 and TRAIL-R3 expression in
1046 metastatic colorectal carcinomas. *Eur J Cancer* **44**, 2312-2318 (2008).
- 1047 81. Abbas, T. & Dutta, A. p21 in cancer: intricate networks and multiple activities. *Nat Rev*
1048 *Cancer* **9**, 400-414 (2009).
- 1049 82. Ieguchi, K. *et al.* Direct binding of the EGF-like domain of neuregulin-1 to integrins
1050 (alpha6beta3 and alpha6beta4) is involved in neuregulin-1/ErbB signaling. *J Biol Chem*
1051 **285**, 31388-31398 (2010).
- 1052 83. Schosserer, M., Grillari, J. & Breitenbach, M. The Dual Role of Cellular Senescence in
1053 Developing Tumors and Their Response to Cancer Therapy. *Frontiers in oncology* **7**,
1054 278 (2017).
- 1055 84. Schmitt, C.A., Wang, B. & Demaria, M. Senescence and cancer - role and therapeutic
1056 opportunities. *Nature reviews. Clinical oncology* **19**, 619-636 (2022).
- 1057 85. Hernandez-Segura, A. *et al.* Unmasking Transcriptional Heterogeneity in Senescent
1058 Cells. *Curr Biol* **27**, 2652-2660 e2654 (2017).
- 1059 86. Hernandez-Segura, A., Nehme, J. & Demaria, M. Hallmarks of Cellular Senescence.
1060 *Trends Cell Biol* **28**, 436-453 (2018).
- 1061 87. Basisty, N. *et al.* A proteomic atlas of senescence-associated secretomes for aging
1062 biomarker development. *PLoS Biol* **18**, e3000599 (2020).
- 1063 88. Jochems, F. *et al.* The Cancer SENESCopedia: A delineation of cancer cell
1064 senescence. *Cell Rep* **36**, 109441 (2021).

- 1065 89. Fousek, K., Horn, L.A. & Palena, C. Interleukin-8: A chemokine at the intersection of
1066 cancer plasticity, angiogenesis, and immune suppression. *Pharmacol Ther* **219**,
1067 107692 (2021).
- 1068 90. Cambier, S., Gouwy, M. & Proost, P. The chemokines CXCL8 and CXCL12: molecular
1069 and functional properties, role in disease and efforts towards pharmacological
1070 intervention. *Cell Mol Immunol* **20**, 217-251 (2023).
- 1071 91. Hoffmann, E., Dittrich-Breiholz, O., Holtmann, H. & Kracht, M. Multiple control of
1072 interleukin-8 gene expression. *J Leukoc Biol* **72**, 847-855 (2002).
- 1073 92. Ortiz-Montero, P., Londono-Vallejo, A. & Vernet, J.P. Senescence-associated IL-6 and
1074 IL-8 cytokines induce a self- and cross-reinforced senescence/inflammatory milieu
1075 strengthening tumorigenic capabilities in the MCF-7 breast cancer cell line. *Cell*
1076 *Commun Signal* **15**, 17 (2017).
- 1077 93. Li, A., Dubey, S., Varney, M.L., Dave, B.J. & Singh, R.K. IL-8 directly enhanced
1078 endothelial cell survival, proliferation, and matrix metalloproteinases production and
1079 regulated angiogenesis. *J Immunol* **170**, 3369-3376 (2003).
- 1080 94. Tobin, R.P. *et al.* IL-6 and IL-8 Are Linked With Myeloid-Derived Suppressor Cell
1081 Accumulation and Correlate With Poor Clinical Outcomes in Melanoma Patients.
1082 *Frontiers in oncology* **9**, 1223 (2019).
- 1083 95. Li, J. *et al.* Transcriptional Profiling Reveals the Regulatory Role of CXCL8 in Promoting
1084 Colorectal Cancer. *Front Genet* **10**, 1360 (2019).
- 1085 96. Bie, Y. *et al.* The Crucial Role of CXCL8 and Its Receptors in Colorectal Liver
1086 Metastasis. *Dis Markers* **2019**, 8023460 (2019).
- 1087 97. Czajka-Francuz, P. *et al.* Serum cytokine profile as a potential prognostic tool in
1088 colorectal cancer patients - one center study. *Rep Pract Oncol Radiother* **25**, 867-875
1089 (2020).
- 1090 98. Jin, W.J., Xu, J.M., Xu, W.L., Gu, D.H. & Li, P.W. Diagnostic value of interleukin-8 in
1091 colorectal cancer: a case-control study and meta-analysis. *World J Gastroenterol* **20**,
1092 16334-16342 (2014).
- 1093 99. Patsouras, M.D., Karagianni, P., Kogionou, P. & Vlachoyiannopoulos, P.G. Differential
1094 CpG methylation of the promoter of interleukin 8 and the first intron of tissue factor in
1095 Antiphospholipid syndrome. *J Autoimmun* **102**, 159-166 (2019).
- 1096 100. Hanahan, D. Hallmarks of Cancer: New Dimensions. *Cancer Discov* **12**, 31-46 (2022).
- 1097 101. Machon, C. *et al.* Study of intracellular anabolism of 5-fluorouracil and incorporation in
1098 nucleic acids based on an LC-HRMS method. *J Pharm Anal* **11**, 77-87 (2021).
- 1099 102. Martin, M. Cutadapt removes adapter sequences from high-throughput sequencing
1100 reads. *EMBnet j.* **17**, 10 (2011).
- 1101 103. Dobin, A. *et al.* STAR: ultrafast universal RNA-seq aligner. *Bioinformatics* **29**, 15-21
1102 (2013).
- 1103 104. Liao, Y., Smyth, G.K. & Shi, W. featureCounts: an efficient general purpose program
1104 for assigning sequence reads to genomic features. *Bioinformatics* **30**, 923-930 (2014).
- 1105 105. Love, M.I., Huber, W. & Anders, S. Moderated estimation of fold change and dispersion
1106 for RNA-seq data with DESeq2. *Genome Biol* **15**, 550 (2014).
- 1107 106. Benjamini, Y. & Hochberg, Y. Controlling the False Discovery Rate: A Practical and
1108 Powerful Approach to Multiple Testing. *Journal of the Royal Statistical Society. Series*
1109 *B (Methodological)* **57**, 289-300 (1995).
- 1110 107. McKinney, W. Data Structures for Statistical Computing in Python, in *Proceedings of*
1111 *the 9th Python in Science Conference*. (ed. S.v.d.W.a.J. Millman) (2010).
- 1112 108. Mudunuri, U., Che, A., Yi, M. & Stephens, R.M. bioDBnet: the biological database
1113 network. *Bioinformatics* **25**, 555-556 (2009).
- 1114 109. Kolberg, L., Raudvere, U., Kuzmin, I., Vilo, J. & Peterson, H. gprofiler2 -- an R package
1115 for gene list functional enrichment analysis and namespace conversion toolset
1116 g:Profiler. *F1000Res* **9** (2020).
- 1117 110. Klopfenstein, D.V. *et al.* GOATOOLS: A Python library for Gene Ontology analyses.
1118 *Sci Rep* **8**, 10872 (2018).

- 1119 111. Liberzon, A. *et al.* The Molecular Signatures Database (MSigDB) hallmark gene set
1120 collection. *Cell Syst* **1**, 417-425 (2015).
- 1121 112. Hunter, J.D., Vol. 9 90-95 (IEEE Computer Society, 2007).
- 1122 113. Waskom, M. seaborn: statistical data visualization. *Journal of Open Source Software*
1123 **6**, 3021 (2021).
- 1124 114. Fernandez, N.F. *et al.* Clustergrammer, a web-based heatmap visualization and
1125 analysis tool for high-dimensional biological data. *Sci Data* **4**, 170151 (2017).
- 1126 115. Adler, D., Nenadi, O. & Zucchini, W. Rgl: A r-library for 3d visualization with opengl.
1127 (2003).
- 1128 116. Hu, Y. & Smyth, G.K. ELDA: extreme limiting dilution analysis for comparing depleted
1129 and enriched populations in stem cell and other assays. *J Immunol Methods* **347**, 70-
1130 78 (2009).
- 1131
- 1132

1133 **Figure legends**

1134

1135 **Figure 1. 5-FU induces cancer cell plasticity**

1136 **a**, Histogram comparing untreated (CTRL) and 5-FU-treated cell proliferation, by analysis of
1137 live HCT-116 and HT-29 cell numbers, showing mean \pm SD for the indicated time points.
1138 Experiments were performed in triplicate; **** or ##### $p < 0.0001$, *** $p < 0.001$, ## $p < 0.01$, one-
1139 way Anova test. Stars indicate p values comparison with time zero and hash signs for treated
1140 vs. untreated.

1141 **b**, Analysis of total HCT-116 and HT-29 cell numbers during 5-FU treatment (D1, D2 or D3)
1142 and after 5-FU withdrawal (D7). Mean \pm SD. Experiments were performed in triplicate; ****
1143 $p < 0.0001$, two-way Anova test.

1144 **c**, Percentage of caspase 3-expressing HCT-116 cells, measured by flow cytometry, before
1145 treatment (D0) and at indicated time points. Mean \pm SD. Experiments were performed in
1146 triplicate; *** $p < 0.001$, one-way Anova test.

1147 **d**, Overexpression of GFP^{high} CRC cells treated at the indicated time points, measured by
1148 FACS as fold increase normalized to untreated cells (D0, CTRL=1). Mean \pm SD. Experiments
1149 were performed in triplicate.

1150 **e**, Overexpression of GFP^{high} cells in CRC xenografts from mice, being treated (5-FU), or not
1151 (CTRL), measured by FACS, as percentage of GFP^{high} cells. Means are represented.
1152 Experiments were performed in triplicate.

1153 **f-h**, Assessment of cell reprogramming by 5-FU. **(f)** Schematic representation of reporter
1154 system for lineage-tracing. CRC cells, containing the pGreenZeo plasmid, are transduced with
1155 pLenti-EIF1 α AmCyan (AmCyan cells) or pLenti-EIF1 α mCherry (mCherry cells).
1156 GFP^{low}AmCyan cells and GFP^{high}mCherry cells are sorted, pooled, and treated with DMSO
1157 (CTRL) or 5-FU. FACS analysis of GFP^{high} cells discriminates between enrichment and
1158 reprogramming (increase of mCherry population and AmCyan population respectively). **(g-h)**
1159 Percentage of GFP^{high}AmCyan and of GFP^{high}mCherry HCT-116 **(g)** and HT-29 **(h)** cells either
1160 untreated (CTRL) or treated with 5-FU (5-FU) and quantified by FACS, showing mean \pm SD.
1161 Experiments were performed in triplicate; *** $p < 0.001$, two-way Anova test).

1162 See also Extended Data Fig. 1.

1163

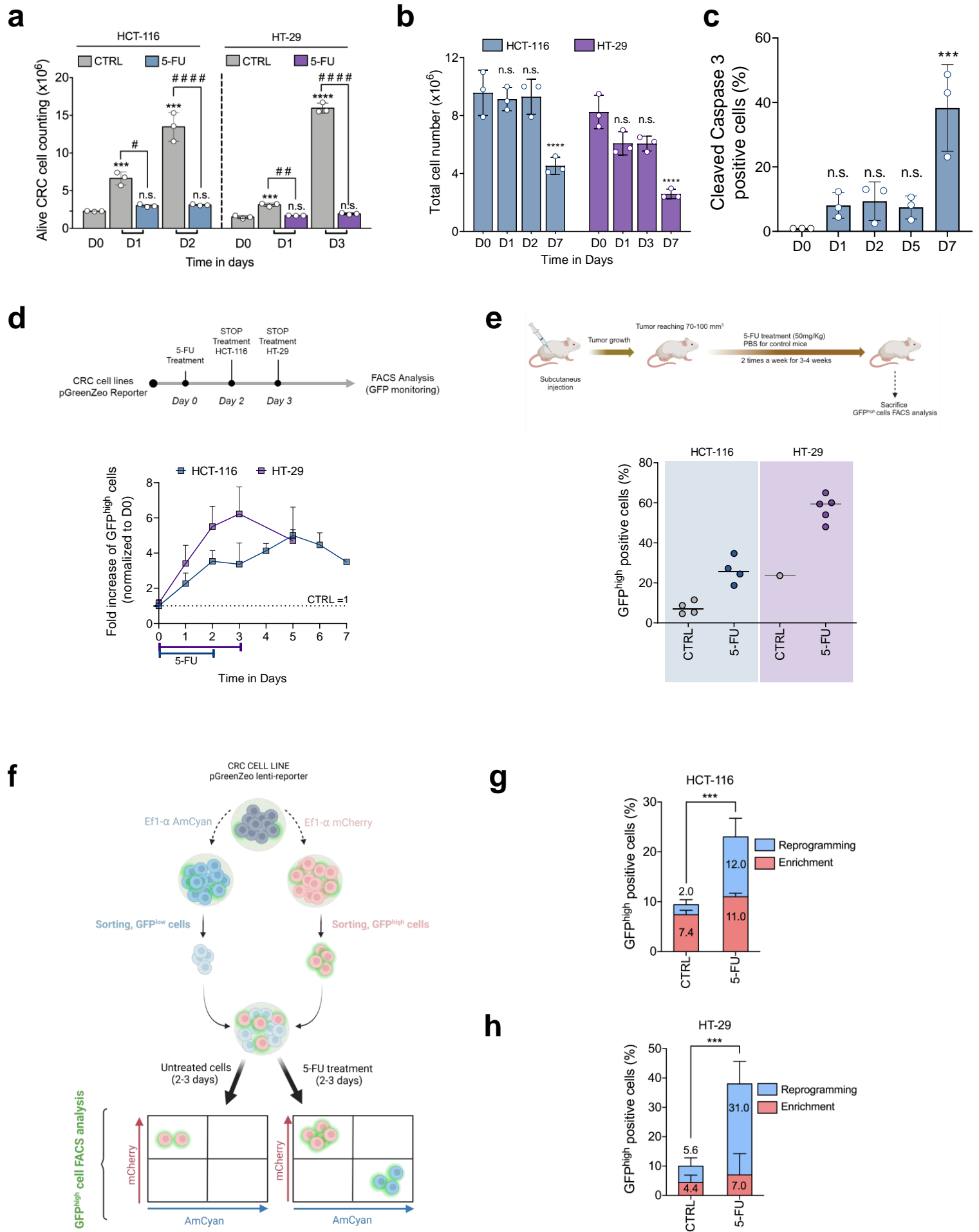


Fig. 1

1164
1165
1166
1167
1168
1169
1170
1171
1172
1173
1174
1175
1176
1177
1178
1179
1180
1181
1182
1183

Figure 2. 5-FU reshapes the translational program

a, 5-FU incorporation into rRNA assessed using liquid chromatography coupled with high resolution mass spectrometry (LC-HRMS) and measured as the number of 5-FU molecules *per* ribosome in HCT-116 and HT-29 cells at the indicated time points, showing mean \pm SD. Experiments were performed in triplicate; **** $p < 0.0001$, *** $p < 0.001$, ** $p < 0.01$, difference with time zero by unpaired Students t-test.

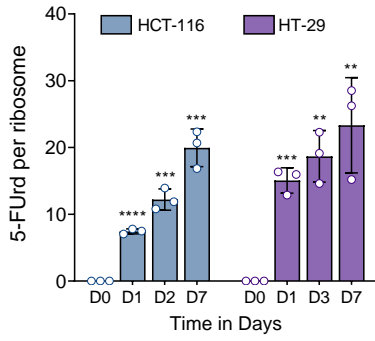
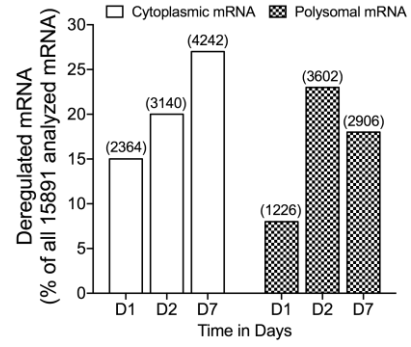
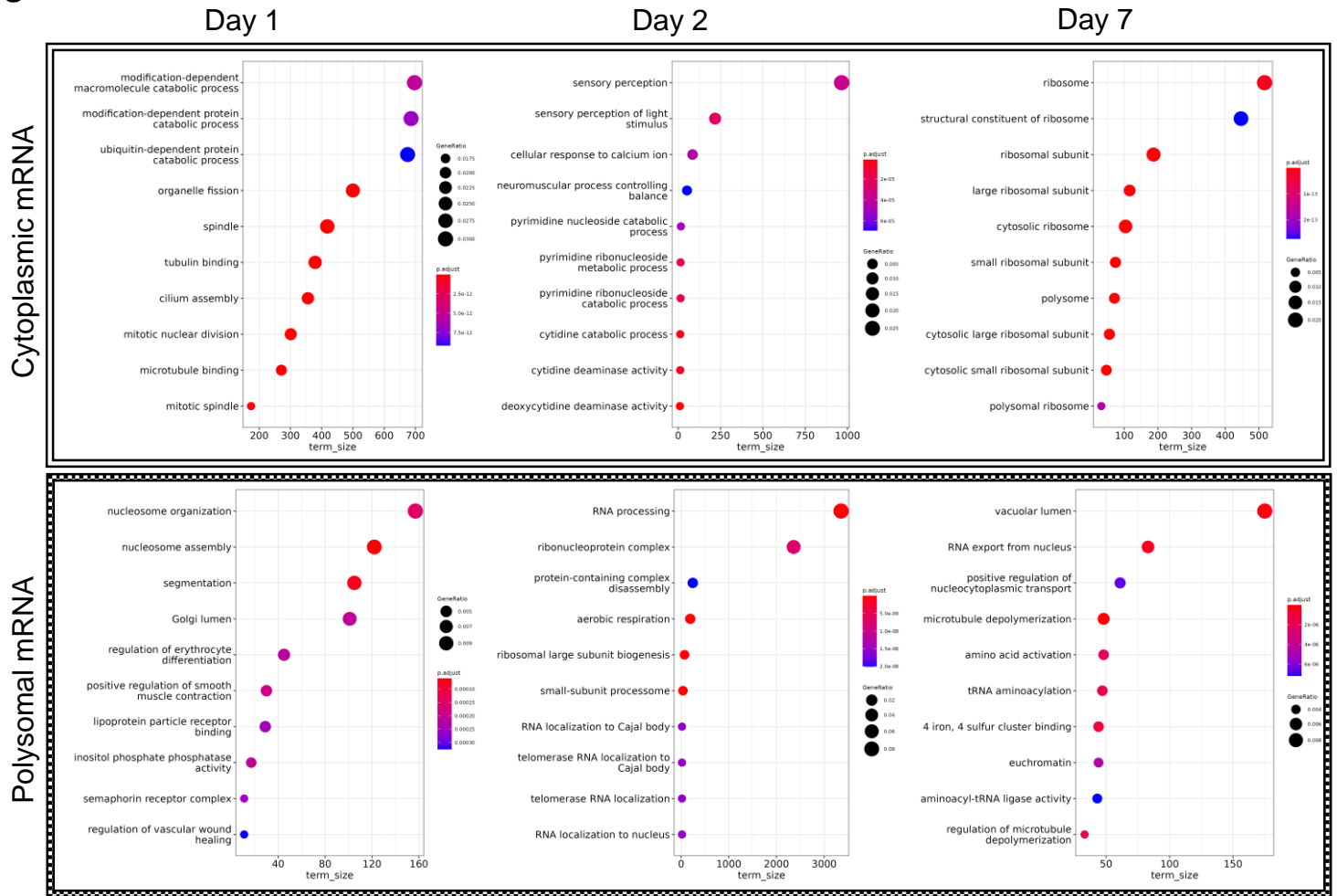
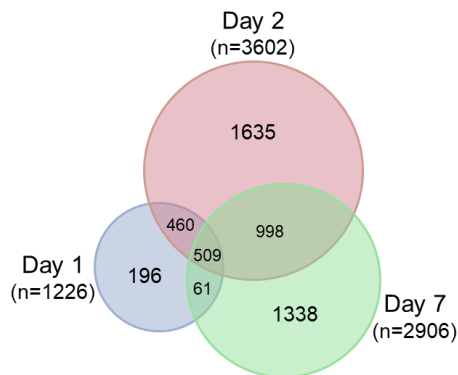
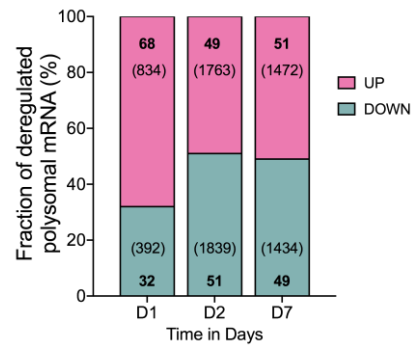
b, Percentage of RNA differently present in cytoplasm (cytoplasmic mRNA) or associated with polysomes (polysomal mRNA) at D1, D2 and D7 compared with D0 in HCT-116 cells. Corresponding number of RNA are shown between brackets.

c, Top ten Gene ontology (GO) gene-sets enriched in HCT-116 cells at D1, D2 and D7 compared with D0 specific to cytoplasmic mRNA (upper panel) and polysomal mRNA (lower panel). NES: normalized enrichment score.

d, Venn diagram showing the comparison of the polysomal RNA differently associated with polysomes at D1, D2 and D7 compared with D0 in HCT-116 cells. n: total number of deregulated genes at indicated time point.

e, Percentage of RNA whose association with polysomes is either increased (UP) or decreased (DOWN) at D1, D2 and D7 compared with D0 in HCT-116 cells.

See also Extended Data Fig. 2.

a**b****c****d****e****Fig. 2**

1184
1185
1186
1187
1188
1189
1190
1191
1192
1193
1194
1195
1196
1197

Figure 3. 5-FU modifies translome of epigenetic regulator genes

a, Heatmap representing 124 epigenetic regulator genes (ERGs) that are deregulated at the translational level at least at one time point D1, D2 and D7, in HCT-116 cells. Red is up, blue is down. P-value of the three respective conditions (p-adj) <0.05 is indicated by black squares.

b, Venn diagram showing the intersection of deregulated ERGs at the translational level at D1, D2 and D7 in HCT-116 cells. For the detailed list of genes see [Extended Data Table 1](#).

c, Venn diagram showing the intersection of upregulated (UP) and downregulated (DOWN) ERGs at the translational level at D1, D2 and D7 in HCT-116 cells. Deregulated RNA specific to D7 are indicated below. For the detailed list of genes see [Extended Data Table 2](#) and [Table 3](#) respectively.

d, Western blot analysis of HDAC9 and HDAC6 before treatment (D0) and at indicated time point in HCT-116 cells, with H3 as the loading control.

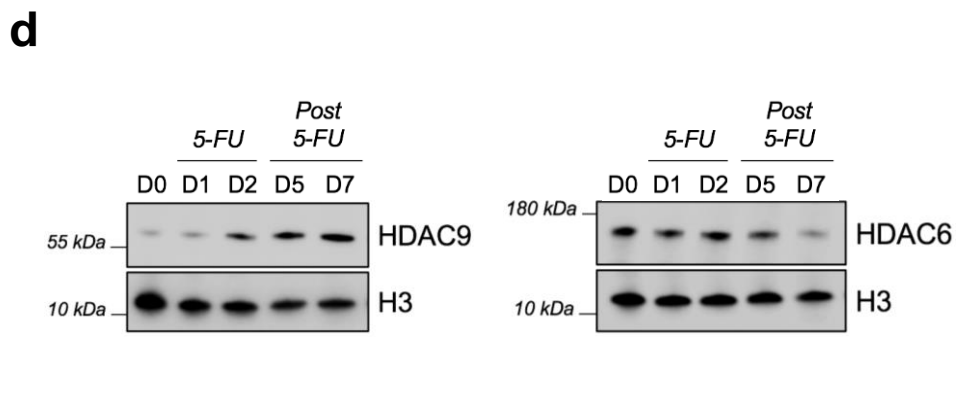
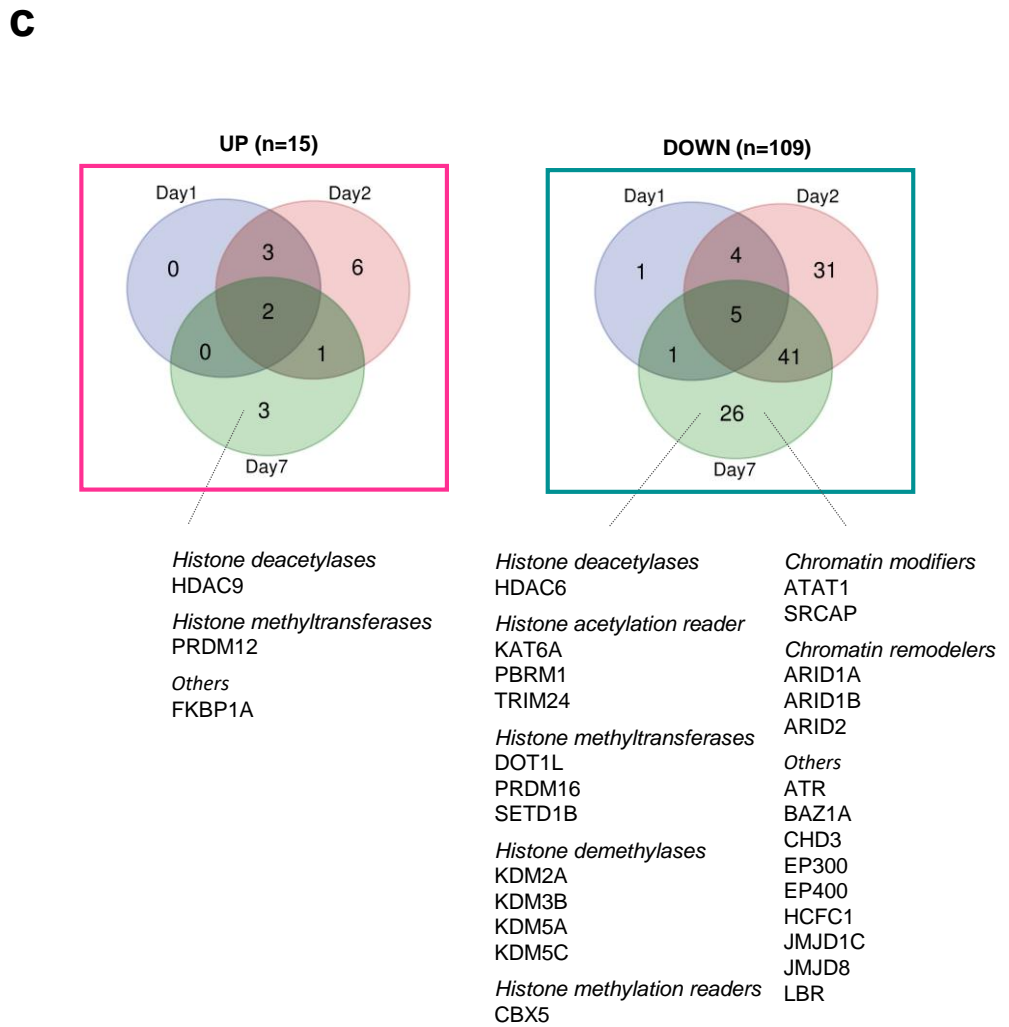
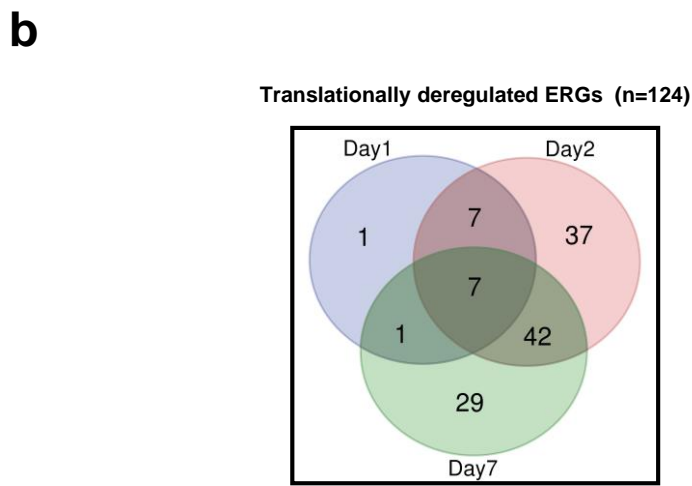
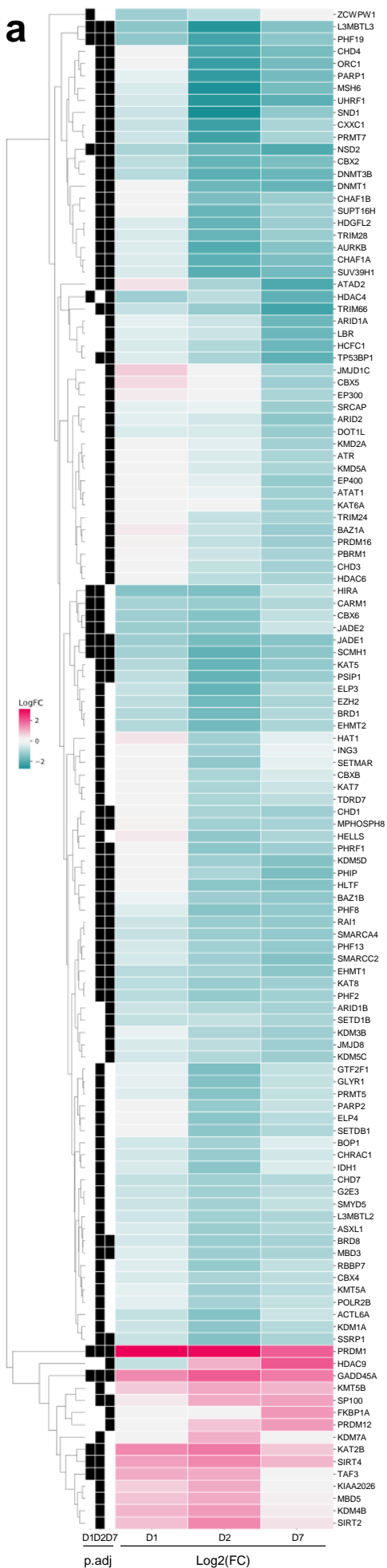


Fig. 3

1198
1199
1200
1201
1202
1203
1204
1205
1206
1207
1208
1209
1210
1211
1212
1213
1214
1215
1216
1217
1218

Figure 4. 5-FU induces translational programs for apoptosis and cell cycle arrest

a, Histogram representing the eight genes implicated in cell death that are upregulated at the translational level at all time points D1, D2 and D7.

b-c, Western blot analysis of the indicated cell death-associated proteins in HCT-116 (**b**) and HT-29 (**c**) cells before treatment (D0) and at the indicated time points, with H3 as the loading control.

d-g, Cell cycle alteration of HCT-116 (**d-e**) and HT-29 (**f-g**) cells by 5-FU treatment. Flow cytometry analysis (**d** and **f**). Grey curves, D0 cycle; Colored curves, D1 to D7 cycles of HCT-116 (blue) and HT-29 (purple). (**e** and **g**) percentage of cell cycle distribution before treatment (D0) and at indicated times.

h, Gene set enrichment analysis (GSEA) of translationally deregulated genes implicated in cell cycle in treated cells at D7 time point (compared with untreated cells (D0)). NES: normalized enrichment score; FDR-p: false discovery rate.

i, Western blot analysis of the cycle regulators in HCT-116 cells before treatment (D0) and at the indicated time points, with H3 as the loading control.

j-k, Western blot analysis of the level of phosphorylated H3 and of P21 in HCT-116 (**j**) and HT-29 (**k**) cells, before treatment (D0) and at the indicated time points, with H3 as the loading control.

See also Extended Data Fig. 3.

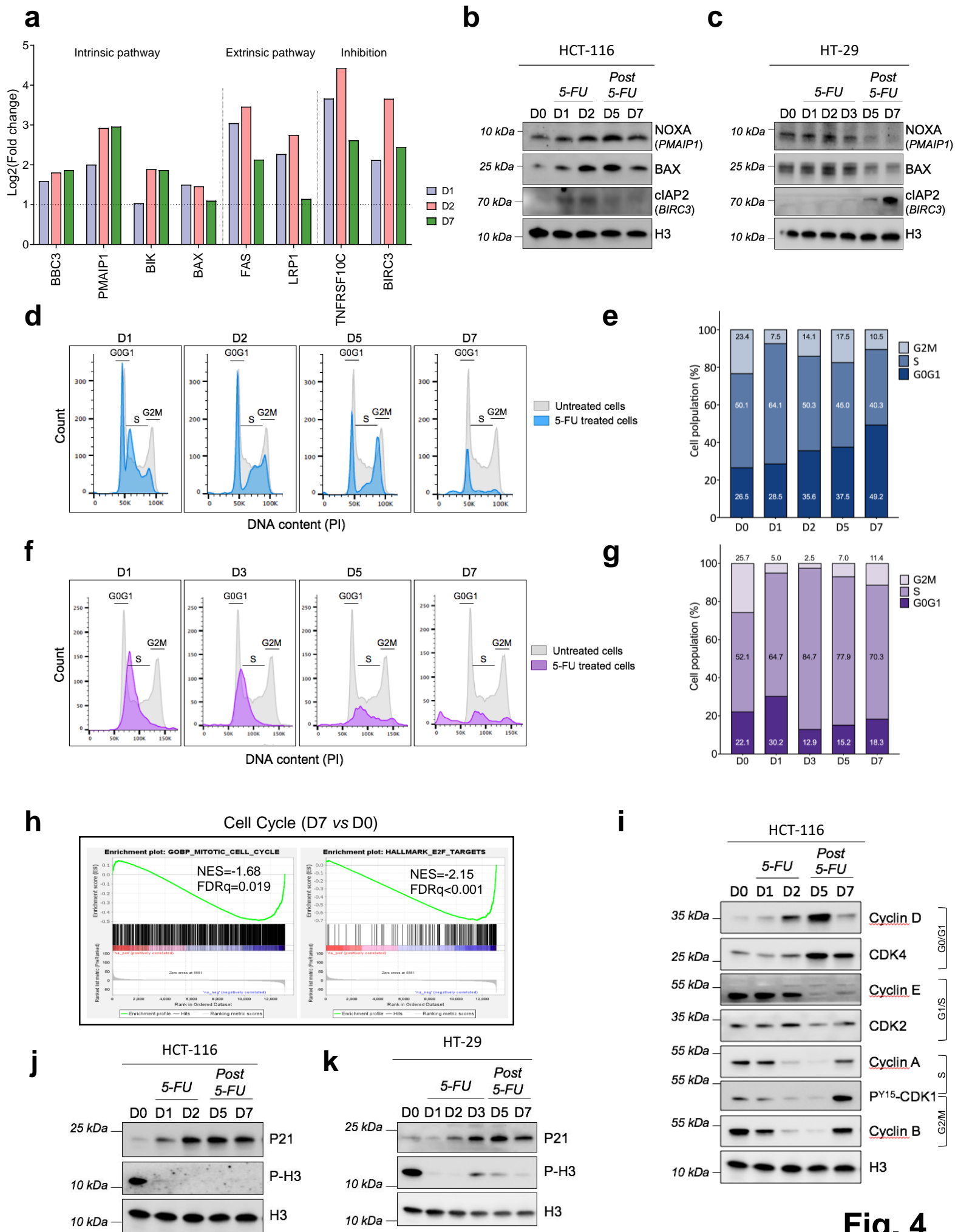


Fig. 4

1219
1220
1221
1222
1223
1224
1225
1226
1227
1228
1229
1230
1231
1232
1233
1234
1235
1236
1237

Figure 5. 5-FU translational control induces senescence and promotes the SASP

a-b, Increased SA-beta-gal activity following 5-FU treatment of HCT-116. Representative images of bright field and SA-beta-Gal staining of HCT-116 cells (**a**) and percentage of HCT-116 cells staining positive for SA-beta-Gal (**b**) before treatment (D0) and after 5-FU withdrawal (D7), showing mean \pm SD. Experiments were performed in triplicate; **** $p < 0.0001$, two-way Anova test. Scale bar, 50 μ m.

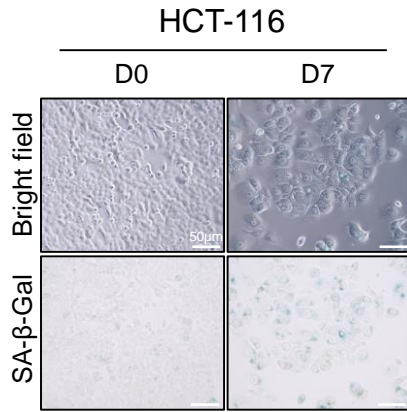
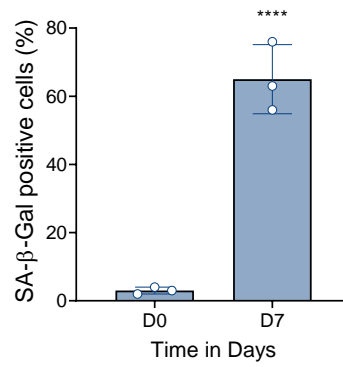
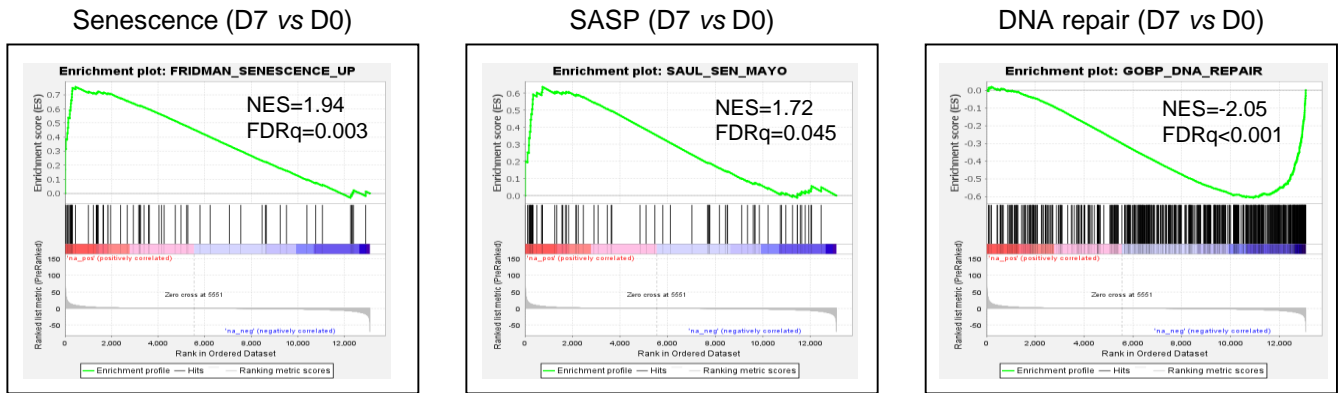
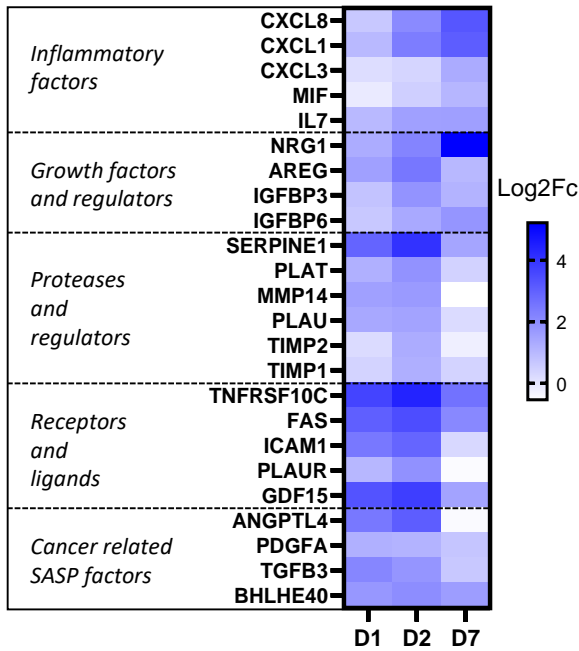
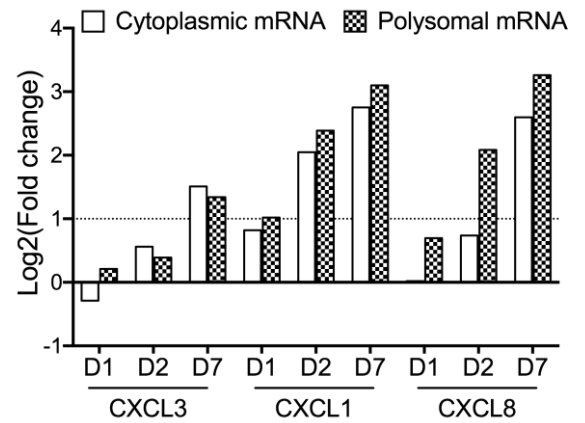
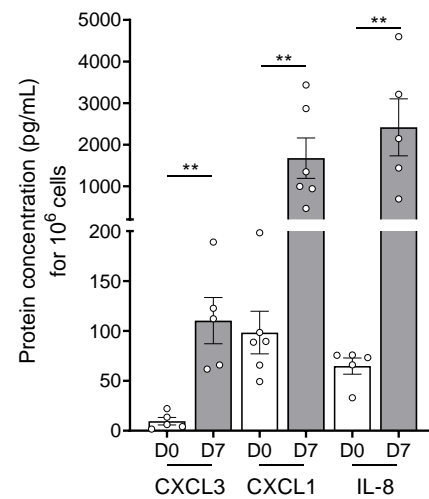
c, Gene set enrichment analysis (GSEA) of translationally deregulated genes implicated in senescence, SASP and DNA repair in treated cells at D7 time point (compared with untreated cells (D0)). NES: normalized enrichment score; FDR-p: false discovery rate.

d, Heatmap representing relative fold-enrichment, compared to D0, of SASP genes that are upregulated at any of the three time points D1, D2 or D7.

e, Analysis of the presence of mRNAs encoding CXCL1, CXCL3 and IL-8 inflammatory cytokines in cytoplasm and in polysomes at indicated times.

f, Inflammatory cytokine CXCL1, CXCL3 and IL-8 expression in supernatant harvested from treated HCT-116 cells at D7 compared with untreated cells, determined by ELISA, showing mean \pm SD. Experiments were performed in triplicate; ** $p < 0.01$; unpaired Students t-test.

See also Extended Data Fig. 4.

a**b****c****d****e****f****Fig. 5**

1238
1239
1240
1241
1242
1243
1244
1245
1246
1247
1248

Figure 6. IL-8 overexpression imparts protumoral capacities to persist cells

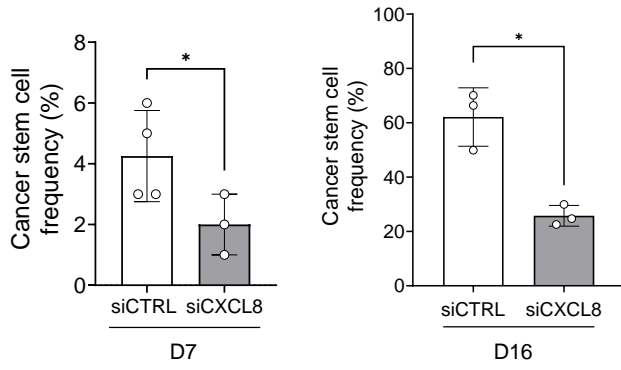
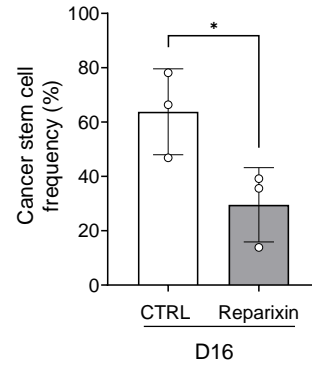
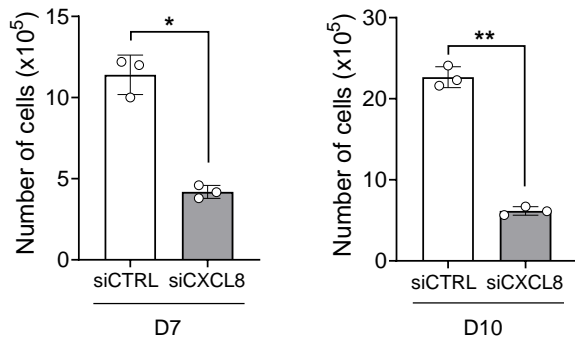
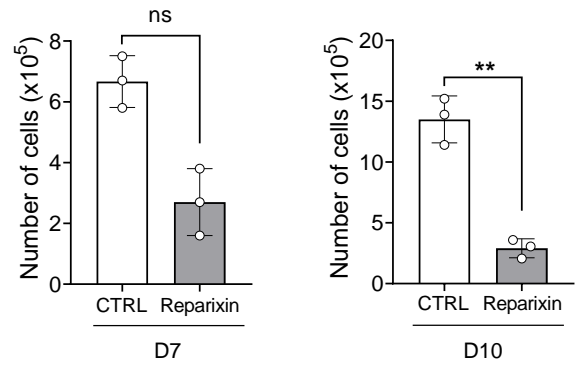
a-b, Decrease of sphere frequency in 5-FU treated HCT-116 cells under inactivation of CXCL8, using **(a)** siRNA targeting CXCL8 or **(b)** IL-8 receptor inhibitor reparixin, showing mean \pm SD.

Experiments were performed in triplicate; * $p < 0.05$; paired Students t-test.

c-d, Decreased viability of 5-FU treated HCT-116 cells under inactivation of CXCL8, using siRNA targeting **(c)** CXCL8 or **(d)** IL-8 receptor inhibitor reparixin, showing mean \pm SD.

Experiments were performed in triplicate; * $p < 0.05$; ** $p < 0.01$; paired Students t-test.

See also Extended Data Fig. 5.

a**b****c****d****Fig. 6**

1249 **Acknowledgments**

1250 We thank Julian Venables for editing the manuscript, Joanna Czarnecka-Herok for her
1251 technical help for the characterization of the senescence phenotype of cells, Karen Mahtouk
1252 for her constructive discussion, Pierre Martinez for his advice on R coding, the Flow Cytometry
1253 Core Facility of CRCL, the ATGC bioinformatics platform of the LIRMM for computing services
1254 (ATGC is part of IFB and France Génomique networks), the Montpellier Genomix
1255 (<http://www.mgx.cnrs.fr>) sequencing facility. This work was supported by the "Fondation ARC
1256 pour la Recherche sur le Cancer" PGA for the project TRANSLATOL
1257 N°ARCPGA12021020003052_3561 (for J.-J.D., J.P. and E.R.), the Institut National du Cancer
1258 (INCA) PLBIO for the projects FluoRib N°2018-131 (for J.-J.D., J.P., J.G., and E.R.), the
1259 LYriCAN INCa-DGOS-Inserm_12563 and LYriCAN+ INCa-DGOS-INSERM-ITMO
1260 cancer_18003 (for J.-J.D., N.D.V., Z.H., and R.K.), the Ligue contre le cancer comité de la
1261 Loire (for J.K.), the Ligue Contre le Cancer (for E.S., D.B. and N.M.), the Institut Convergence
1262 PLAsCAN, F-69373, Lyon, France (for J.-J.D., A.V., D.B., and N.M.) and the Dev2Can Labex
1263 Laboratory, 69373 Lyon, France (for J.-J.D.). This publication is based upon work from COST
1264 Action TRANSLACORE CA21154, supported by COST (European Cooperation in Science and
1265 Technology). M.C.-D. was supported by Fondation ARC pour la Recherche sur le Cancer and
1266 Fondation de France.

1267 Disclaimer: Where authors are identified as personnel of the International Agency for Research
1268 on Cancer/World Health Organization, the authors alone are responsible for the views
1269 expressed in this article and they do not necessarily represent the decisions, policy, or views
1270 of the International Agency for Research on Cancer/World Health Organization.

1271

1272

1273 **Author contributions**

1274 M.C.-D., O.V., J.R., A.V., T.F., R.K., L.J., J.T., A.C., C.M., C.B., J.V., L.L., C.M., and N.M.
1275 performed experiments. M.C.-D., O.V., J.R., A.V., C.M, J.G., A.D., Z.H., D.B., and N.M.
1276 designed experiments. M.C.-D., O.V., J.R., A.V., T.F., R.K., J.K., F.C., A.V., E.S., C.M, and
1277 N.M. analyzed data. E.R., N.D.V., J.P., and J.-J.D. designed and supervised the study. E.R.,
1278 N.D.V., J.P., and J.-J.D. wrote the manuscript.

1279

1280 **Declaration of interests**

1281 The authors declare no competing interests.

1282

1283 **Additional information**

1284 Extended Data: Extended Data Fig. 1-5 and Extended Data Table 1-4.

1285 Supplemental Information: Supplemental Table 1-3.

1286

1287

1288